Journal of Nanobiotechnology

RESEARCH

Open Access

MSCs-EVs harboring OA immune memory reprogram macrophage phenotype via modulation of the mt-ND3/NADH-CoQ axis for OA treatment

Jingdi Zhan[1,2], Jing Zou[1,2], Qiming Pang[1,2], Zhuolin Chen[1,2], Junyan Liu[1,2], Senrui Liu[1,2], Chengcheng Du[1,2], Jiacheng Liu[1,2], Weikang Zhao[1,2*], Lili Dong[1,2*] and Wei Huang[1,2*]

Abstract

Background Osteoarthritis (OA) is a prevalent degenerative joint disease and current therapies are insufficient to halt its progression. Mesenchymal stem cells-derived extracellular vesicles (MSCs-EVs) offer promising therapeutic potential for OA treatment, and their efficacy can be enhanced through strategic engineering approaches.

Methods Inspired by the immune memory of the adaptive immune system, we developed an engineered strategy to impart OA-specific immune memory to MSCs-EVs. Using Luminex technology, inflammatory factors (IFN-γ, IL-6, and TNF-α), which mimic the OA inflammatory microenvironment, were identified and used to prime MSCs, generating immune memory-bearing MSCs-EVs (iEVs). Proteomic analysis and complementary experiments were conducted to evaluate iEVs' effects on macrophage phenotypic reprogramming.

Results iEVs, particularly IL-6-EV, exhibited potent immunoregulatory functions along with the ability to modulate mitochondrial metabolism. Both in vitro and in vivo, IL-6-EV significantly reprogrammed macrophages towards the M2 subtype, effectively suppressing articular inflammation and OA progression. Mechanistic studies revealed that IL-6-EV facilitated M2 polarization by regulating mitochondrial oxidative phosphorylation via the mt-ND3/NADH-CoQ axis.

Conclusion This study introduces a strategy to enhance MSCs-EVs' therapeutic efficacy in OA. Multi-omics analysis and biological validation demonstrate its potential, providing new insights for MSCs-EVs' future application in OA and other clinical conditions.

Keywords MSCs-derived extracellular vesicles, Engineered, Macrophages, Mitochondria metabolism, mt-ND3, Osteoarthritis

*Correspondence:
Weikang Zhao
weikangzhao90@hospital.cqmu.edu.cn
Lili Dong
dllbme@alu.cqu.edu.cn
Wei Huang
huangwei68@263.net

Full list of author information is available at the end of the article

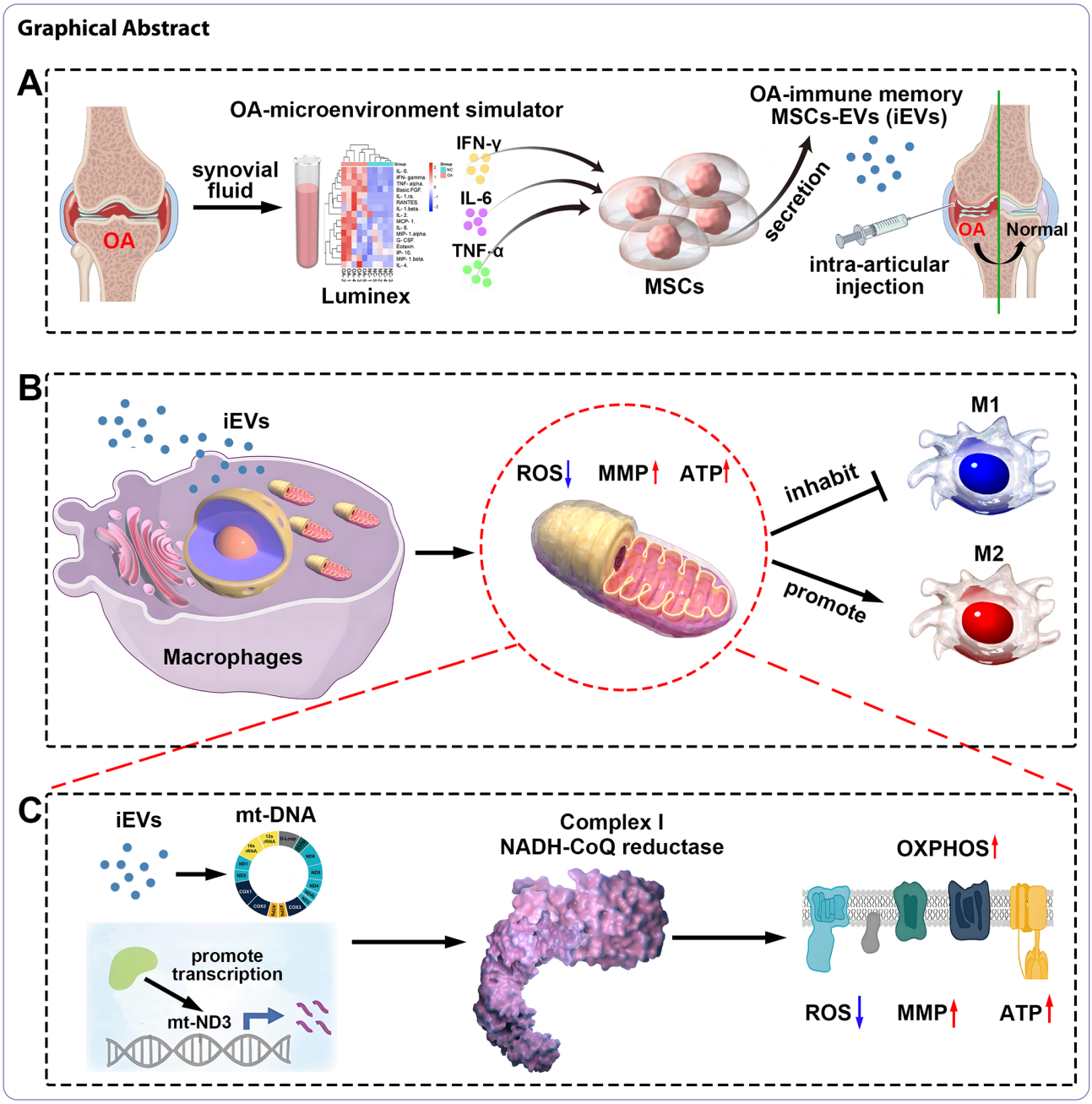

Introduction

Osteoarthritis (OA) represents a significant global health challenge, affecting over 240 million individuals worldwide [1]. OA is one of the fastest-growing causes of disability worldwide [2]. Despite the high prevalence and disability burden of OA, no effective methods currently exist to halt its progression. Therefore, exploring potential therapeutic strategies based on the pathological mechanisms of OA is imperative.

Macrophage-mediated synovitis plays a pivotal role in the initiation and progression of OA [3, 4]. Previous studies conducted by our group have demonstrated a significant elevation in the M1/M2 macrophage ratio in both the synovium and synovial fluid of OA patients, with this ratio being closely associated with the severity of the disease [5]. Modulating the polarization of M1 macrophages toward the M2 phenotype has been shown to significantly ameliorate OA progression [6].

In recent years, numerous studies have highlighted the potential of extracellular vesicles derived from mesenchymal stem cells (MSCs-EVs) in promoting M2 macrophage polarization and alleviating OA progression [7, 8]. However, the ability of MSCs-EVs to regulate macrophage polarization is closely linked to the condition of

the parent cells. For instance, EVs derived from MSCs of young donors exhibit potent immunomodulatory properties, whereas EVs derived from older donors display significantly diminished immunosuppressive capacity [9]. Furthermore, the immunomodulatory capacity of mesenchymal stem cells is not inherent, but is acquired by the stimulation of multiple inflammatory factors in the inflammatory microenvironment. In response to different inflammatory stimuli, MSCs acquire distinct immunophenotypes and activate different signaling pathways that may regulate immune responses differently [10–12].

This may account for the suboptimal immunoregulatory effects of MSCs-EVs in certain studies. Consequently, researchers have explored various strategies to enhance the therapeutic efficacy of MSCs-EVs in OA. For instance, 3D cultivation has been shown to improve the efficacy of EVs in OA [13], while hypoxia preconditioning enhances EVs-driven reprogramming of M2 macrophages [14]. Although these strategies have shown some progress, the preconditioning factors often lack direct relevance to OA, contributing to the heterogeneity observed in EVs treatment outcomes. Moreover, most studies have focused on the impact of preconditioning strategies on the therapeutic potential of MSCs-EVs, with limited evidence regarding how these strategies influence the composition of EVs. This may represent another factor contributing to the heterogeneity in treatment outcomes. This heterogeneity inevitably hinders the clinical application of MSCs-EVs, necessitating that future research focus on enhancing MSCs-EVs efficacy while minimizing this variability.

Under physiological conditions, MSCs exist in a quiescent state [15]. However, when their microenvironment is altered, both the content and function of the EVs secreted by MSCs undergo corresponding changes [16]. This responsiveness of MSCs-EVs to external stimuli parallels the adaptive immune system's defense responses to foreign invaders. When the adaptive immune system encounters stimuli such as viruses and bacteria, it generates immune memory through processes such as antigen presentation, leading to the secretion of specific antibodies that allow the body to combat these threats more rapidly and effectively [17]. Inspired by this phenomenon of immune memory, we hypothesized that MSCs might exhibit a comparable "immune memory" mechanism. Specifically, when MSCs are exposed to external stimuli, the changes in the EVs they secrete are not nonspecific but represent targeted responses to the stimuli, thereby endowing MSCs-EVs with specific "immune memory". For instance, a study by Yuki Nakao et al. demonstrated that MSCs-EVs treated with pro-inflammatory factors exhibited stronger anti-inflammatory effects [18]. Furthermore, compared to EVs derived from resting MSCs, EVs derived from IL-1β-preactivated MSCs can more effectively reprogram pro-inflammatory macrophages into anti-inflammatory phenotypes [19]. Our previous research also demonstrated that MSCs-EVs preconditioned with IFN-γ exhibited stronger anti-inflammatory effects in both in vitro and in vivo OA models [20]. However, the design of the preconditioning strategies in these studies was non-specific and not directly related to the diseases under study. Based on these findings, we propose an innovative strategy to optimize the therapeutic efficacy and reduce the heterogeneity of MSCs-EVs: preconditioning MSCs with disease-related stimuli to generate EVs that possess "immune memory" specific to those stimuli, thereby enhancing their effectiveness in promoting tissue repair in specific diseases.

On the other hand, although numerous studies have reported that MSCs-EVs can regulate the balance of macrophage polarization [21, 22], the underlying mechanisms remain unclear. Mitochondria are central to cellular metabolism, providing energy, participating in biosynthesis, maintaining redox balance, and acting as platforms for various immune signaling pathways [23]. A study has shown that anti-inflammatory macrophages in the later stages of inflammation contain more mitochondria than early-stage pro-inflammatory counterparts [24]. Furthermore, in M1 macrophages, mitochondrial oxidative phosphorylation (OXPHOS) is impaired, accompanied by a decrease in membrane potential and reduced ATP production, while ROS levels are elevated, all of which hinder the transition to the M2 phenotype [25, 26]. These findings suggest that mitochondria play a critical role in macrophage phenotypic alterations. Based on these findings, we hypothesized that MSCs-EVs may influence macrophage polarization by regulating mitochondrial metabolism.

To explore the potential and mechanisms of OA-specific immune memory MSCs-EVs (iEVs) for modulating macrophage polarization and treating OA inflammation, we first examined the cytokines in the joint fluid of OA patients and screened out three highly enriched inflammatory factors (IFN-γ, IL-6, and TNF-α), which were used to prime MSCs to obtain immune-engineered EVs. Proteomic analyses and complementary experiments revealed the molecular signature and immunoregulatory capabilities of iEVs. Multi-omic approaches were then employed to investigate the underlying molecular mechanisms of immunoregulation. The results demonstrated that iEVs enhance mitochondrial energy metabolism in M1 macrophages by regulating the mt-ND3/NADH-CoQ axis, thereby reprogramming them to the M2 phenotype. This, in turn, reduces chondrocyte inflammation and inhibits OA progression. In summary, MSCs-EVs endowed with OA-specific immune memory show significant therapeutic potential for OA, offering new insights into their application in treating OA and other diseases.

Materials and methods

MSCs culture and MSCs-EVs isolation from conditioned medium

Mouse MSCs(C3H/10T1/2) were purchased from Pricella Biotechnology (Wuhan, China). IFN-γ, IL-6 and TNF-α were obtained from MedChemExpress (Shanghai, China). MSCs were maintained in the MEM-α medium supplemented with 10% fetal bovine serum (FBS) and 1% penicillin/streptomycin (P/S) at 37 °C in 5% CO_2, with medium changes every 2 days. MSCs-EVs were isolated as previously described [20]. Briefly, we first screened for the three inflammatory factors IFN-γ, IL-6, and TNF-α by Luminex assay. MSCs were then cultured in conditioned medium containing IFN-γ, IL-6, and TNF-α at concentrations of 0, 20, 50, 100, 200, and 500 ng/mL for 48 h. Subsequently, the cells were incubated in EVs-free medium for additional 48 h to allow for EVs secretion. The conditioned medium was then collected and centrifuged at 1,000 g for 10 min to remove cellular debris; The supernatant was collected and large particles were removed by centrifugation at 10,000 g for 30 min; Finally, the supernatant was filtered through a 0.22 μm membrane and ultracentrifuged at 120,000 g for 2 h to collect MSCs-EVs (CON-EV, IFN-γ-EV, IL-6-EV, and TNF-α-EV). The protein content of MSCs-EVs (1 × 10^8 particles) was quantified by BCA Protein Assay Kit (Beyotime, Shanghai, China). Furthermore, the protein expressions of CD9, CD63, CD81, and COX IV in MSCs-EVs were assessed by Western Blot.

Transmission electron microscopy (TEM) analysis of MSCs-EVs

For TEM analysis, a 10 μL aliquot of the vesicle suspension was placed onto a carbon-coated copper grid and allowed to adsorb for 5 min. Excess liquid was wicked away with filter paper. The grid was then negatively stained with 2% uranyl acetate for 1 min to enhance contrast. After drying, the grid was examined under a transmission electron microscope (JEOL JEM-2000FX) at an accelerating voltage of 80 kV. Images were captured to document the morphology and size of the extracellular vesicles.

Nanoparticle tracking analysis (NTA) of MSCs-EVs

We measured the exosome particle size and concentration using nanoparticle tracking analysis (NTA) at VivaCell Biosciences with ZetaView PMX 110 (Particle Metrix, Meerbusch, Germany) and corresponding software ZetaView 8.04.02. The isolated extracellular vesicle samples were appropriately diluted using phosphate-buffered saline (PBS) to measure the particle size and concentration. NTA measurements were recorded and analyzed at 11 positions. The ZetaView system was calibrated using 110 nm polystyrene particles. Temperature was maintained around 23 °C to 30 °C.

MSCs-EVs proteomic sequencing and data analysis

We used Tandem Mass Tag (TMT) labeling quantitative proteomics technology to analyze the MSCs-EVs samples (CON-EV, IFN-γ-EV, IL-6-EV, and TNF-α-EV), exploring the protein composition, expression differences, and corresponding biological functions. We revealed protein types and analyzed differentially expressed proteins in MSCs-EVs using Principal Component Analysis (PCA) and Subcellular localization. Gene Ontology (GO) and Kyoto Encyclopedia of Genes and Genomes pathway (KEGG) enrichment analyses were performed using a p-value < 0.05 as the exclusion criterion.

Uptake of MSCs-EVs by RAW264.7

MSCs-EVs were labeled with the red fluorescent dye DiI (Beyotime, China). The labeled MSCs-EVs were co-cultured with RAW264.7 macrophages for 24 h at 37 °C in 5% CO_2. After the co-culture, the cells were fixed with 4% paraformaldehyde. Nuclei were stained with DAPI (Beyotime, China). Finally, the uptake of MSCs-EVs was visualized and captured with a fluorescence microscope (Olympus, Japan).

Identification of macrophage polarization

RAW264.7 macrophages were purchased from Pricella Biotechnology (Wuhan, China) and cultured in DMEM medium. Lipopolysaccharide (LPS) was purchased from MedChemExpress(Shanghai, China) and utilized to induce macrophages polarization towards M1 phenotype (200ng/mL for 12 h). Afterward, the culture medium was replaced with fresh DMEM medium containing CON-EV or IL-6-EV (3 × 10^8 particles/mL). After 48 h of culture, the cells were collected and subjected to immunofluorescence and qPCR analysis to assess the expression levels of CD86, CD206, ARG-1, iNOS, IL-6, TNF-α, IL-1β, and IL-10. The primer sequences are provided in Table S1 (Supplementary Material).

Detection of mitochondrial morphology and function in macrophages

Macrophages from various groups were collected and subjected to fixation, embedding, and sectioning, followed by observation of mitochondrial morphology using transmission electron microscopy. Mitochondrial membrane potential was assessed using the JC-1 assay kit (Beyotime, China), while ATP production was quantified using an enhanced ATP detection kit (Beyotime, China). ROS levels were evaluated using the DCFH-DA probe (Beyotime, China).

The interaction between macrophages and chondrocytes

Following the previously described method [27], primary chondrocytes were isolated from the knee joint cartilage of C57BL/6 mice. After the induction of inflammation in chondrocytes with IL-1β (20ng/mL, 24 h) in vitro, macrophages from different groups were co-cultured with the chondrocytes using the transwell system. Immunofluorescence and Western blot analyses were subsequently conducted to examine the expression of type II collagen (COL II), ADAMTS5, Cleaved-caspase3 (C-caspase3), and MMP13 in the chondrocytes.

RNA sequencing of macrophages and complementary experiments

RAW264.7 macrophages were cultured in DMEM medium. LPS was used to induce macrophages polarization towards M1 phenotype (200ng/mL for 12 h). The culture medium was then replaced with fresh DMEM medium containing IL-6-EV (3 × 10^8 particles/mL) or IL-4 (20ng/mL). After 48 h of culture, total RNA from macrophages (LPS, IL-6-EV, IL-4) was isolated and purified using TRIzol (Beyotime, China). Sequencing was performed using the Illumina NovaSeqTM 6000 (LC Bio Technology, Hangzhou, China) with standard operating procedures for paired-end sequencing, with a sequencing mode of PE150. The sequencing data were filtered to yield high-quality sequencing data (Clean Data) which underwent an analysis using R programming language. Differentially expressed genes (DEGs), with a p-value < 0.05 and fold change > 2, were identified. The identified DEGs were subjected to enrichment analyses for functional annotations in GO and signal pathways in KEGG. The gene expressions of mt-ND1, mt-ND2 and mt-ND3 were detected by qPCR. The protein expression of mt-ND3 was assessed using both immunofluorescence and Western blot analyses. The primer sequences of mt-ND1, mt-ND2 and mt-ND3 are provided in Table S1 (Supplementary Material).

Detection of oxidative phosphorylation and complex I activity

Western blot analysis was used to detect the protein expression levels of electron transport chain (ETC) Complexes I-V (NDUFB8, SDHB, UQCRC2, MTCO2, and ATP5A), reflecting the oxidative phosphorylation (OXPHOS) status in macrophages. The activity of Complex I was evaluated using the NADH-CoQ reductase activity assay kit (Elabscience, China).

Small interfering RNA (siRNA) transfection

The mt-ND3 siRNA (ND3-si) and negative control siRNA (NC-si) were purchased from Sangon Biotech (Shanghai, China). siRNA transfection was performed using Lipofectamine RNAiMAX (Invitrogen, USA) according to the manufacturer's instructions. After 48 h of siRNA treatment, cells were collected and subjected to qPCR, Western blot, and immunofluorescence analyses to assess the expression levels of mt-ND3, CD86, CD206 and electron transfer chain Complexes I-V. Additionally, ATP production and activity of Complex I were measured. The sequences of mt-ND3-siRNA are listed in Table S2.

Western blot

Protein samples were prepared from cell lysates by lysing cells in RIPA buffer with protease and phosphatase inhibitors. Protein concentration was determined using the BCA Protein Assay Kit (Beyotime, China). Equal amounts of protein (40 μg) were loaded onto a 10% SDS-PAGE gel and separated by electrophoresis at a constant voltage of 120 V for approximately 1 h until the bromophenol blue dye front reached the bottom of the gel. The separated proteins were then transferred to a PVDF membrane. The membrane was blocked with 5% non-fat milk for 1 h at room temperature to prevent non-specific binding. The membrane was incubated overnight at 4 °C with primary antibodies specific to the target proteins (COL II, ADAMTS5, C-caspase3, GAPDH, mt-ND3, NDUFB8, SDHB, UQCRC2, MTCO2, ATP5A, and β-ACTIN, diluted 1:1000). After washing the membrane three times with Tris-buffered saline containing Tween-20 (TBST) for 5 min each, it was incubated with horseradish peroxidase (HRP)-conjugated secondary antibodies (diluted 1:5000) for 1 h at room temperature. The membrane was washed three more times with TBST. Protein bands were detected using an enhanced chemiluminescence (ECL) substrate (Beyotime, China) and visualized using a chemiluminescent imaging system.

Quantitative real-time PCR (qPCR)

Total RNA was extracted from RAW264.7 macrophages in different treatment groups using an RNA extraction kit (Accurate Biology, China) and reverse transcribed into cDNA. qPCR conditions were as follows: 95 °C for 5 min, followed by 40 cycles of 95 °C for 10 s and 60 °C for 30 s. The CFX96 Real-Time PCR System (Bio-Rad, USA) was used for the qPCR reaction. Cycle threshold (Ct) values were obtained and normalized to GAPDH levels. Primer sequences are provided in Table S1.

Immunofluorescence

In brief, the cells underwent the following steps: fixation with 4% paraformaldehyde for 15 min, followed by treatment with 0.1% Triton X-100 at room temperature for 10 min. The 5% goat serum was used to block the cells that were kept in a wet box at 37 °C for 1 h. These were then incubated with primary antibodies overnight at 4 °C in a wet box. After 12 h, the cells were incubated with Alexa Fluor®488- or Alexa Fluor®594-conjugated

secondary antibodies (1:500) at room temperature for 1 h in the dark. Finally, the cell nuclei were stained using DAPI. After each step, the cells were washed with phosphate buffered saline (PBS). After staining, the cells were observed and recorded using a fluorescence microscope (Olympus, Japan).

Animal model of osteoarthritis

The animal study was approved by the Ethics Committee of Chongqing Medical University (Approval Number: IACUC-CQMU-2024-0381). Twenty SD rats were randomly divided into four groups, with 5 rats in each group. Group 1 was the Sham group, which underwent arthrotomy without the surgical manipulation of the anterior cruciate ligament and medial meniscus. Group 2 was the PBS group, which underwent anterior cruciate ligament transection (ACLT) and destabilization of the medial meniscus (DMM), followed by intra-articular injection of PBS solution. The CON-EV group underwent ACLT and DMM procedures, followed by treatment with CON-EV. The IL-6-EV group underwent ACLT and DMM procedures, followed by treatment with IL-6-EV. MSCs-EVs (1×10^{10} particles/mL, 30μL) were injected starting at the fourth week post-surgery, once per week. At the eighth week post-surgery, the rats were euthanized (pentobarbital, 150 mg/kg, intraperitoneal injection), and knee joint specimens were collected for radiological examination.

After fixation with 4% paraformaldehyde, decalcification, and paraffin embedding, the knee joints underwent histological analysis, including staining with hematoxylin and eosin (HE) and Safranin O-fast green on sagittal sections for further evaluation. The severity of OA cartilage damage and synovitis was independently evaluated by three assessors using a modified Mankin scoring system [28] and a synovitis scoring system [29], respectively. Immunohistofluorescence assays were performed to evaluate the expression of MMP13 and Aggrecan in the OA cartilage matrix. Additionally, the expression of IL-6, CD206, iNOS, and mt-ND3 in OA synovium was observed using immunohistofluorescence and immunohistochemical techniques.

Immunohistofluorescence

Tissue sections were initially subjected to antigen retrieval by incubation in citrate antigen retrieval solution (0.01 M, pH 6.0). Subsequent staining procedures followed those used in immunofluorescence. Finally, images were captured using a fluorescence microscope.

Immunohistochemistry

Prior to staining, antigen retrieval was performed by incubating the sections in citrate buffer (pH 6.0) in a pressure cooker for 10 min to expose epitopes. The sections were then cooled at room temperature for 20 min. Endogenous peroxidase activity was blocked by incubating sections in 3% hydrogen peroxide for 10 min. After washing with PBS, sections were treated with a protein blocking solution for 60 min to prevent non-specific binding. The IL-6 primary antibody (1:200) was applied to the sections and incubated overnight at 4 °C. After incubation, the sections were washed with PBS and incubated with a secondary antibody conjugated to horseradish peroxidase for 1 h at room temperature. The sections were then reacted with diaminobenzidine (DAB) and counterstained with hematoxylin. Finally, the stained sections were examined under a light microscope, and images were captured for further analysis.

Statistical analysis

The analysis of the data was done using SPSS 22 and GraphPad Prism 8 software. One-way analysis of variance (ANOVA) was used for data analysis, followed by Tukey's test for group comparisons. The results are presented as mean ± S.D. p-values < 0.05 for were considered statistically significant for differences between groups.

Results

Extraction and identification of MSCs-EVs

Figure 1A presents a schematic representation of the process used to isolate MSCs-EVs. The Luminex assay demonstrated significant upregulation of IFN-γ, IL-6, and TNF-α in the synovial fluid of OA patients (Figure S1). To determine the optimal concentrations of IFN-γ, IL-6, and TNF-α, these inflammatory factors were added to complete culture media at concentrations of 0, 20, 50, 100, 200, and 500 ng/mL, followed by assessment of the total protein and COX IV content in the extracted EVs. Quantitative analysis (Fig. 1B-D) revealed a significant increase in total protein content (1×10^{8} particles) in the IFN-γ (100 ng/mL), IL-6 (50 ng/mL), and TNF-α (50 ng/mL) groups, compared to the control group. Additionally, the levels of COX IV in MSCs-EVs were assessed as an indicator of mitochondrial content. As shown in Figure S2A-C, the protein levels of COX IV in the IFN-γ (100 ng/mL), IL-6 (50 ng/mL), and TNF-α (50 ng/mL) treatment groups were significantly higher than in those treated with other concentrations. Therefore, IFN-γ (100 ng/mL), IL-6 (50 ng/mL), and TNF-α (50 ng/mL) were selected as the optimal concentrations for subsequent experiments. Transmission electron microscopy (TEM) images showed that EVs from all groups exhibited a bilayer, cup-shaped, or oval structure (Fig. 1E), with sizes ranging from 100 to 150 nm. Western blot confirmed the expression of small extracellular vesicle-specific markers, including CD9, CD63, and CD81 (Fig. 1F). Nanoparticle tracking analysis (NTA) showed the peak particle sizes for each group (Fig. 1G). The effects of different inflammatory factors on

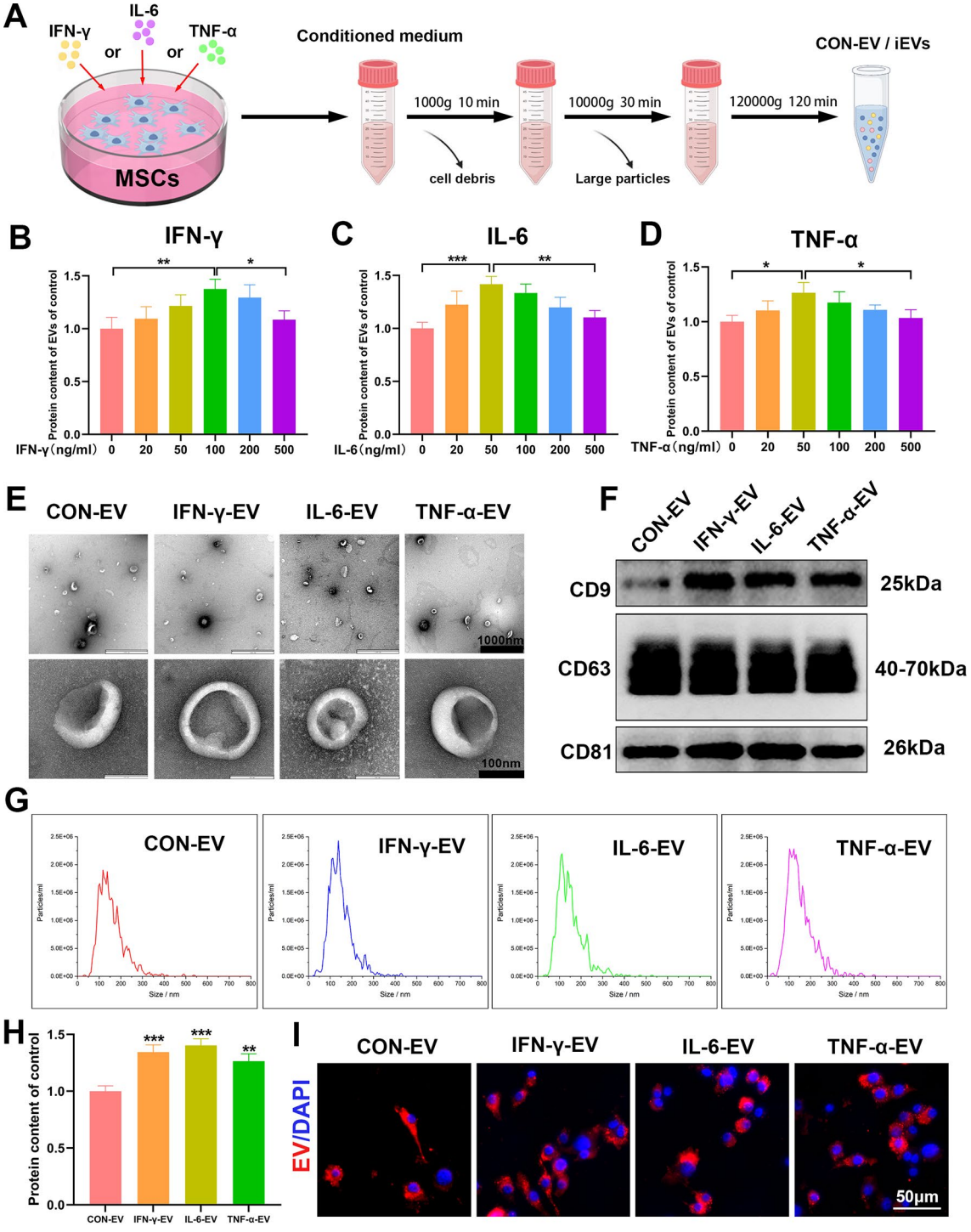

Fig. 1 Characterization of MSCs-EVs with or without preconditioning. (**A**) Schematic of CON-EV, IFN-γ-EV, IL-6-EV and TNF-α-EV extraction. (**B-D**) MSCs-EVs protein content under different concentrations of inflammatory factors (IFN-γ, IL-6, and TNF-α-EV) pretreatment. (**E**) Morphological characteristics of CON-EV, IFN-γ-EV, IL-6-EV and TNF-α-EV under transmission electron microscopy. (**F**) EV-specific protein markers CD9, CD63, and CD81 investigated by Western blot. (**G**) Particle size of various MSCs-EVs. (**H**) The protein content of MSCs-EVs under different inflammatory factors stimulation. (**I**) Labeling of phagocytosed MSCs-EVs by Dil. All data are shown as means ± standard deviations ($n = 3$), *$p < 0.05$, **$p < 0.01$, ***$p < 0.001$, ****$p < 0.0001$

the total protein and COX IV content of EVs were also compared. As shown in Fig. 1H and Figure S2D, all three inflammatory factors increased the total protein and COX IV content of EVs, with the IL-6 treatment group showing the most significant effect. Additionally, fluorescence microscopy demonstrated that DiI-labeled EVs from all groups were engulfed by macrophages, primarily localizing in the cytoplasm (Fig. 1I). These results suggest that preconditioning with these three inflammatory factors increase the total protein and COX IV content of EVs; however, iEVs (IFN-γ-EV, IL-6-EV, TNF-α-EV) do not show significant differences from CON-EV in terms of morphology, size, or internalization.

Analysis of the protein expression profile in iEVs

To explore the compositional and functional changes in MSCs-EVs following stimulation with IFN-γ, IL-6, and TNF-α, we conducted proteomic analysis of the EVs. Principal component analysis (PCA) showed significant compositional differences between IFN-γ-EV, IL-6-EV, TNF-α-EV, and CON-EV (Fig. 2A). Subcellular localization analysis identified the top five proteins identified in the EVs, which included cytoplasmic proteins, nuclear proteins, extracellular proteins, plasma membrane proteins, and mitochondrial proteins (Fig. 2B). Gene Ontology (GO) analysis of IFN-γ-EV demonstrated significant enrichment in biological processes such as ATP binding, mitochondrion, granulocyte chemotaxis and regulation of interleukin-18 production (Fig. 2C). Kyoto Encyclopedia of Genes and Genomes (KEGG) pathway analysis of IFN-γ-EV revealed enrichment in mitochondrial carbohydrate metabolism and immune-related pathways, including the citrate cycle (TCA cycle), pyruvate metabolism, antigen processing and presentation and AMPK signaling pathways (Fig. 2F). GO analysis of IL-6-EV indicated significant enrichment in antioxidant activity, inflammatory response, mitochondrion, and ATP binding (Fig. 2D). KEGG enrichment analysis of IL-6-EV showed involvement in mitochondrial nutrient metabolism and energy metabolism pathways, including pyruvate metabolism, glutathione metabolism, glycolysis/gluconeogenesis and oxidative phosphorylation (Fig. 2G). TNF-α-EV exhibited GO enrichment in NF-kappaB binding, Notch signaling pathway, and regulation of interleukin-8 production, indicating immune-related biological processes (Fig. 2E). KEGG analysis of TNF-α-EV highlighted pathways related to cell proliferation and communication, including DNA replication, ECM-receptor interaction, cell cycle, and PI3K-Akt signaling pathway (Fig. 2H). These results suggest that IFN-γ-EV, IL-6-EV, and TNF-α-EV have the potential to regulate cellular immune processes and mitochondrial metabolism. To further validate the proteomic analysis of iEVs, we treated macrophages with each EV group and assessed M1 and M2 markers using immunofluorescence and qPCR. As shown in Fig. 2I-L, IFN-γ-EV, IL-6-EV, and TNF-α-EV significantly reduced the expression of iNOS in macrophages, while all three iEVs types markedly increased the expression of the M2 marker ARG-1. Notably, qPCR results indicated that, compared with other EVs, IL-6-EV significantly suppressed the expression of iNOS (Figure S3A) and enhanced the expression of ARG-1 (Figure S3B).

IL-6-EV promotes M2 macrophage polarization and mitochondrial function

To further validate the ability of IL-6-EV to regulate macrophage phenotype reprogramming, we assessed pro-inflammatory and anti-inflammatory macrophage markers using immunofluorescence and qPCR. As shown in Fig. 3A and B, lipopolysaccharide (LPS) significantly increased CD86 expression, while CON-EV and IL-6-EV downregulated CD86 expression, with IL-6-EV showing a stronger effect. Additionally, IL-6-EV significantly increased the expression of the M2 macrophage marker CD206 (Fig. 3A and C). qPCR results indicated that IL-6-EV significantly upregulated the gene expression of CD206 and ARG-1, while notably downregulating CD86 and iNOS expression (Fig. 3D). M1 and M2 macrophages play distinct roles in OA by secreting different cytokines. As shown in Fig. 3E, IL-6-EV significantly inhibited the gene expression of pro-inflammatory cytokines TNF-α, IL-6, and IL-1β, while promoting the gene expression of the anti-inflammatory cytokine IL-10.

Additionally, proteomic sequencing analysis of IL-6-EV revealed high enrichment of mitochondrial proteins and related pathways (Fig. 2), and there is a strong relationship between mitochondrial function and macrophage phenotype reprogramming [30]. Therefore, we further investigated the effects of IL-6-EV on macrophage mitochondria. Mitochondrial structure is fundamental to their function. As shown in Fig. 4A, TEM images revealed that the mitochondria in the CON group were elongated or oval-shaped with neatly arranged cristae. In the LPS group, the mitochondria became rounded and swollen, with disrupted cristae. In the CON-EV group, the number of swollen, rounded mitochondria decreased, and their cristae were better organized compared to those in the LPS group. Mitochondria in the IL-6-EV group exhibited structures and cristae similar to those in the CON group. JC-1 assay results indicated that LPS reduced mitochondrial membrane potential, whereas IL-6-EV significantly prevented this LPS-induced decrease (Fig. 4C and D). Additionally, ROS measurements revealed that both CON-EV and IL-6-EV significantly inhibited mitochondrial ROS production (Fig. 4E and F). Similarly, IL-6-EV also showed a significant improvement in mitochondrial ATP production (Fig. 4B). Taken together, LPS disrupted mitochondrial

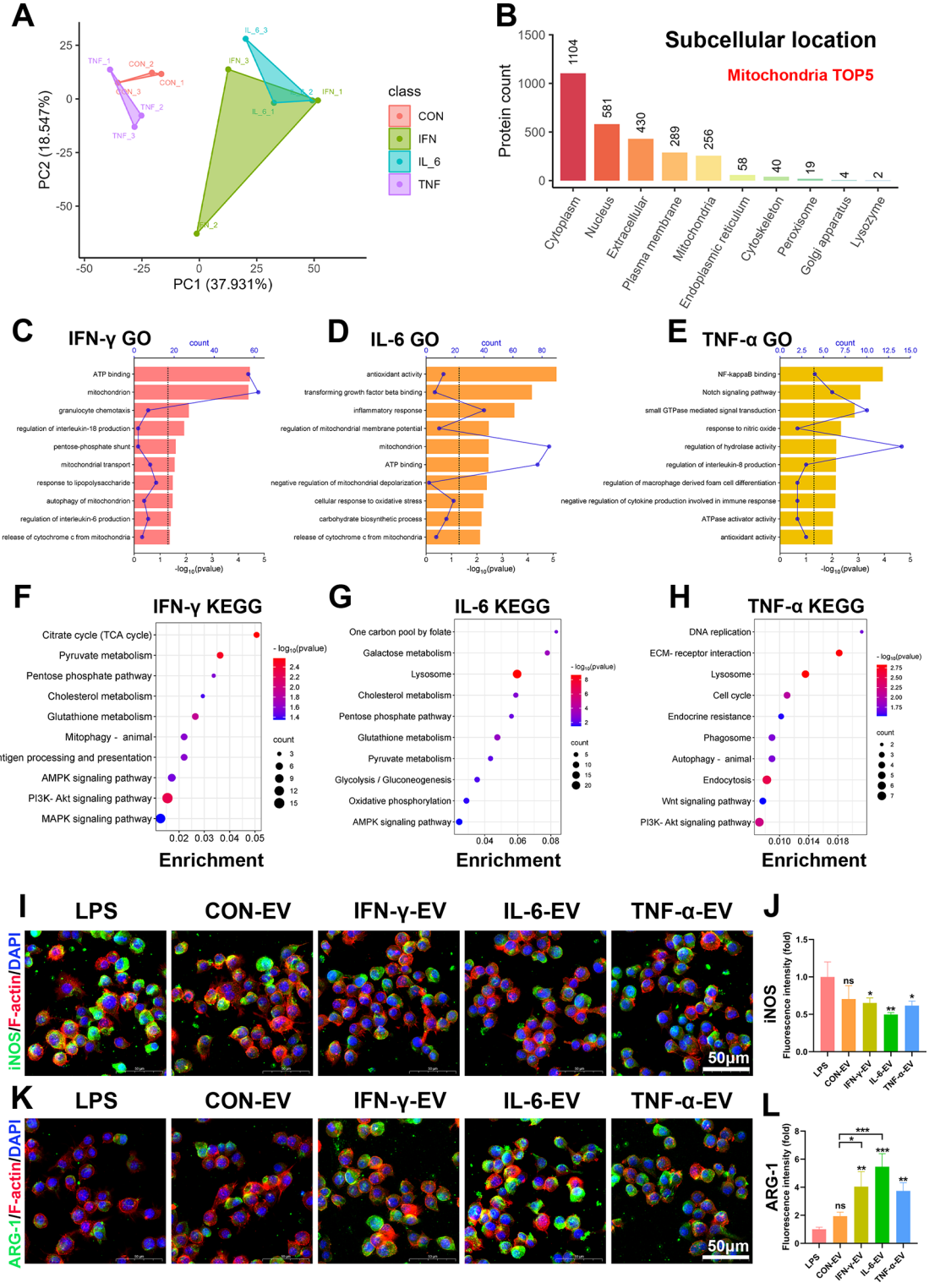

Fig. 2 Proteomic sequencing analysis of CON-EV, IFN-γ-EV, IL-6-EV and TNF-α-EV. (**A**) Principal component analysis of different EVs. (**B**) Subcellular localization of proteins contained in EVs. (**C-E**) GO enrichment analysis of differentially expressed proteins in various EVs. (**F-H**) KEGG enrichment analysis of differentially expressed proteins in various EVs. (**I, J**) Immunofluorescence staining of iNOS in RAW264.7 macrophages and statistical analysis. (**K, L**) Immunofluorescence staining of ARG-1 in RAW264.7 macrophages and statistical analysis. All data are shown as means ± standard deviations ($n = 3$), $^{*}p < 0.05$, $^{**}p < 0.01$, $^{***}p < 0.001$, $^{****}p < 0.0001$

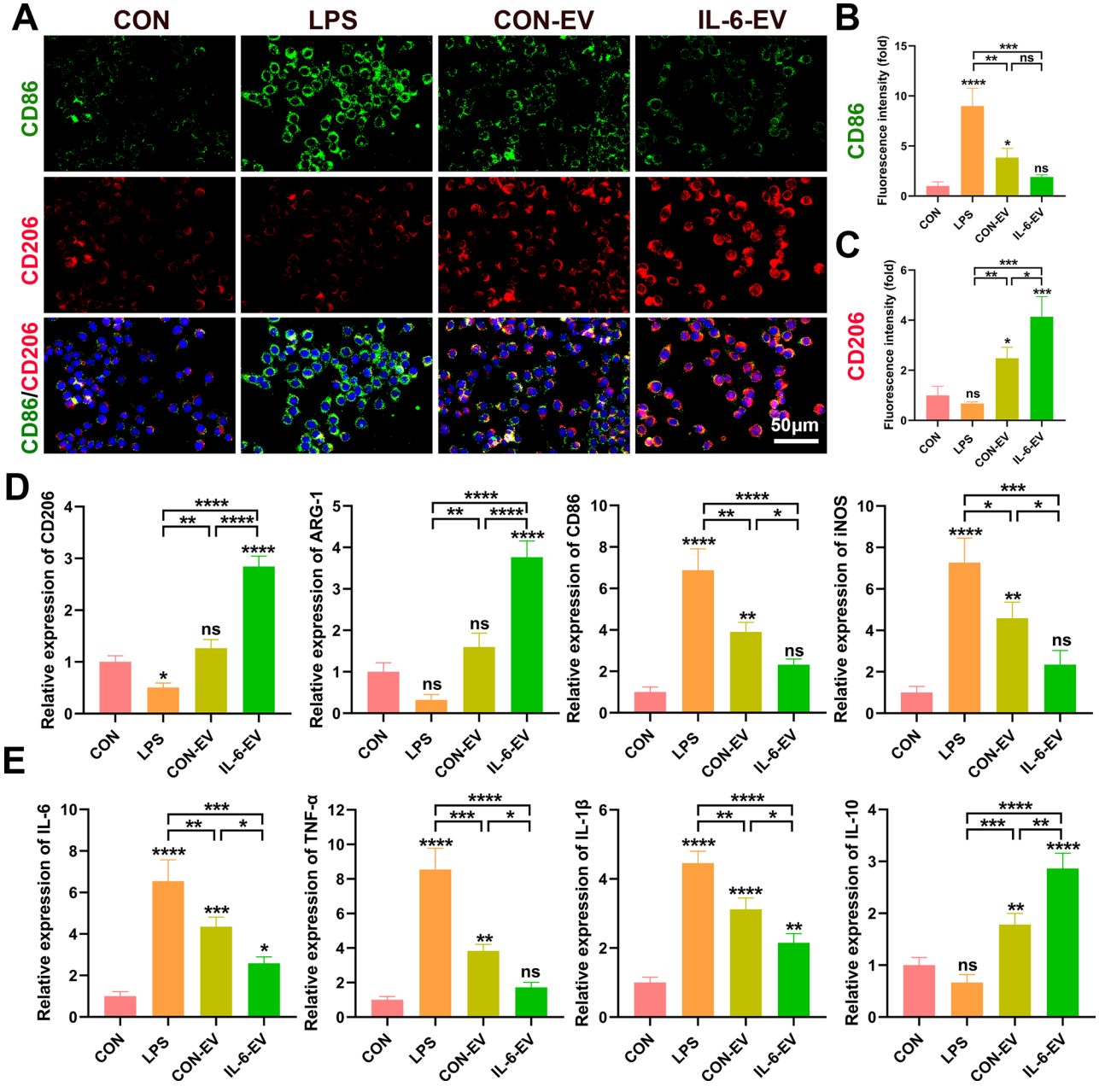

Fig. 3 Effects of CON-EV and IL-6-EV on macrophage phenotype polarization. (**A**) Immunofluorescence detection of M1 macrophage marker (CD86) and M2 macrophage marker (CD206) expression. (**B**) Statistical analysis of fluorescence intensity of CD86 and CD206. (**D**) Gene expression of M1 and M2 macrophages markers (CD206, ARG-1, CD86, and iNOS) was determined using qPCR. (**E**) Gene expression of pro-inflammatory and anti-inflammatory cytokines in macrophages was determined using qPCR. All data are shown as means ± standard deviations ($n = 3$), *$p < 0.05$, **$p < 0.01$, ***$p < 0.001$, ****$p < 0.0001$

morphology, reduced membrane potential, decreased ATP production, and increased ROS generation in macrophages, whereas IL-6-EV demonstrated a strong capacity to positively regulate mitochondrial structure and function. The present findings are consistent with the proteomic sequencing of IL-6-EV shown in Fig. 2, highlighting the substantial potential of IL-6-EV in promoting macrophage polarization to M2 phenotype and improving mitochondrial function.

Macrophages reprogrammed by IL-6-EV improve chondrocytes homeostasis

We first simulated the OA-environment in vitro to assess the impact of IL-6-EV-reprogrammed macrophages on chondrocyte homeostasis using the transwell co-culture system (Fig. 5A). Primary mouse chondrocytes were isolated, and the characterization results confirmed their typical chondrocyte features (Fig. 5B). Western blot analysis revealed that IL-1β treatment significantly reduced

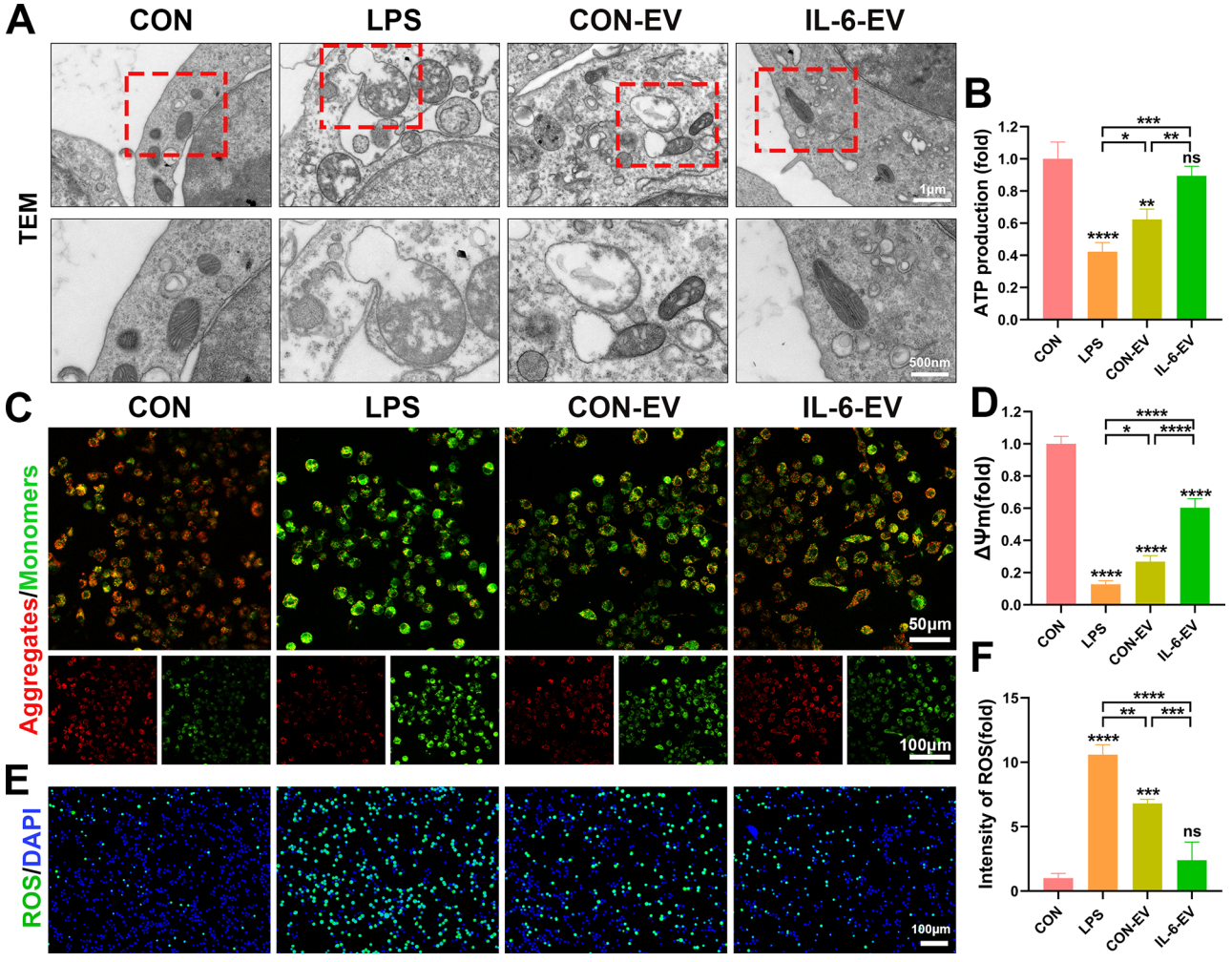

Fig. 4 Effects of CON-EV and IL-6-EV on the morphology and function of mitochondria in macrophages. (**A**) The morphology of mitochondria observed by transmission electron microscopy. (**B**) ATP production of mitochondria under different treatments. (**C**) JC-1 staining of mitochondria and (**D**) statistical analysis of mitochondrial membrane potential. (**E**) ROS levels detected by DCFH-DA probe. (**F**) Statistical analysis of ROS levels. All data are shown as means ± standard deviations ($n = 3$), $^{*}p < 0.05$, $^{**}p < 0.01$, $^{***}p < 0.001$, $^{****}p < 0.0001$

the expression of COL II, while promoting the expression of ADAMTS5 and C-caspase3 compared to the control group (Fig. 5C). In contrast, treatment with IL-1β + CON-EV-M2 and IL-1β + IL-6-EV-M2 significantly increased the expression of COL II in chondrocytes, with levels rising by 1.73-fold and 2.96-fold, respectively, compared to the IL-1β group (Fig. 5D). Additionally, the levels of ADAMTS5 in the IL-1β + CON-EV-M2 and IL-1β + IL-6-EV-M2 groups were 58% and 21% of those observed in the IL-1β group, respectively (Fig. 5E). The protein levels of C-caspase3 in the IL-1β + CON-EV-M2 and IL-1β + IL-6-EV-M2 groups was also reduced to 68% and 37% of the IL-1β group, respectively (Fig. 5F). Furthermore, immunofluorescence results (Fig. 5G-J) demonstrated that MMP13 expression was significantly reduced in the IL-1β + IL-6-EV-M2 group, while COL II expression was increased, consistent with the Western blot findings. These results suggest that IL-6-EV-reprogrammed M2 macrophages significantly restore homeostatic balance in inflammatory chondrocytes.

Analysis of macrophage RNA sequencing

To investigate the mechanisms by which IL-6-EV regulates macrophage polarization, we conducted RNA sequencing of macrophages. PCA revealed significant differences among macrophages treated with IL-6-EV, LPS, and IL-4. (Figs. 6 A and S4). The volcano plot of differentially expressed genes showed that 550 genes were significantly downregulated and 1,094 genes were significantly upregulated in the IL-6-EV group (Fig. 6B). Previous proteomic analysis of IL-6-EV showed that these vesicles contain proteins involved in regulating mitochondrial metabolic pathways. Furthermore, our biological experiments confirmed that IL-6-EV promotes M2 macrophage polarization and enhances mitochondrial structure and function. Based on our findings and

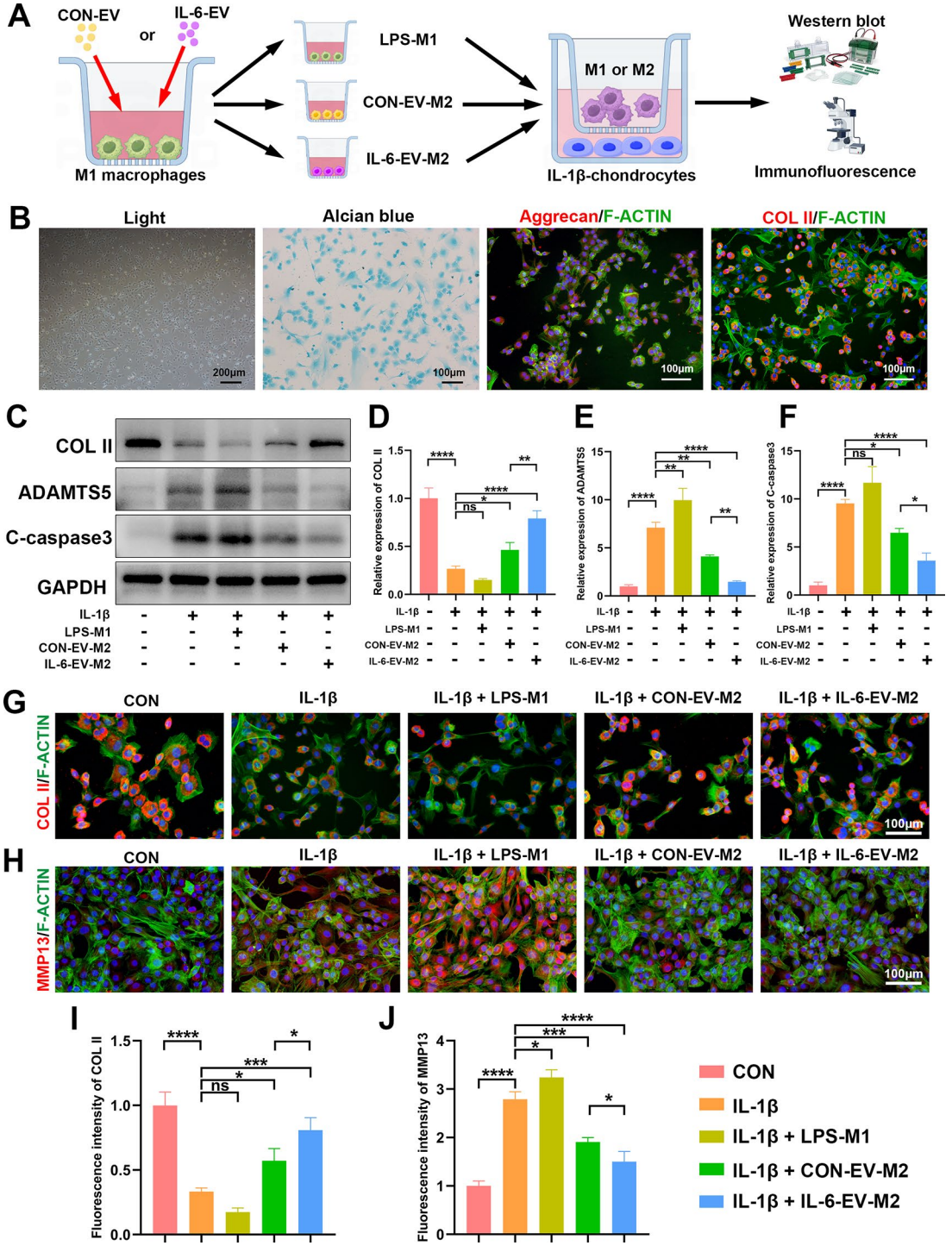

Fig. 5 Crosstalk of reprogrammed macrophages on chondrocytes. (**A**) Schematic illustration of the co-culture model featuring macrophages and chondrocytes. (**B**) Identification of primary chondrocytes. (**C**) COL II, ADAMTS5, and C-caspase3 among various groups investigated by Western blot. (D-F) Statistical analysis of COL II, ADAMTS5, and C-caspase3. (**G, H**) COL II and MMP13 among various groups investigated by Immunofluorescence staining and (I, J) statistical analysis of them. All data are shown as means ± standard deviations ($n = 3$), $^{*}p < 0.05$, $^{**}p < 0.01$, $^{***}p < 0.001$, $^{****}p < 0.0001$

reports from other studies [30], we hypothesized that IL-6-EV promotes M2 polarization by modulating mitochondrial oxidative phosphorylation (OXPHOS). Therefore, we present the expression of OXPHOS proteins enriched in IL-6-EV proteome sequencing via a cluster heatmap (Fig. 6C). We then generated a Venn diagram to intersect the differentially expressed genes from RNA sequencing with oxidative phosphorylation gene sets

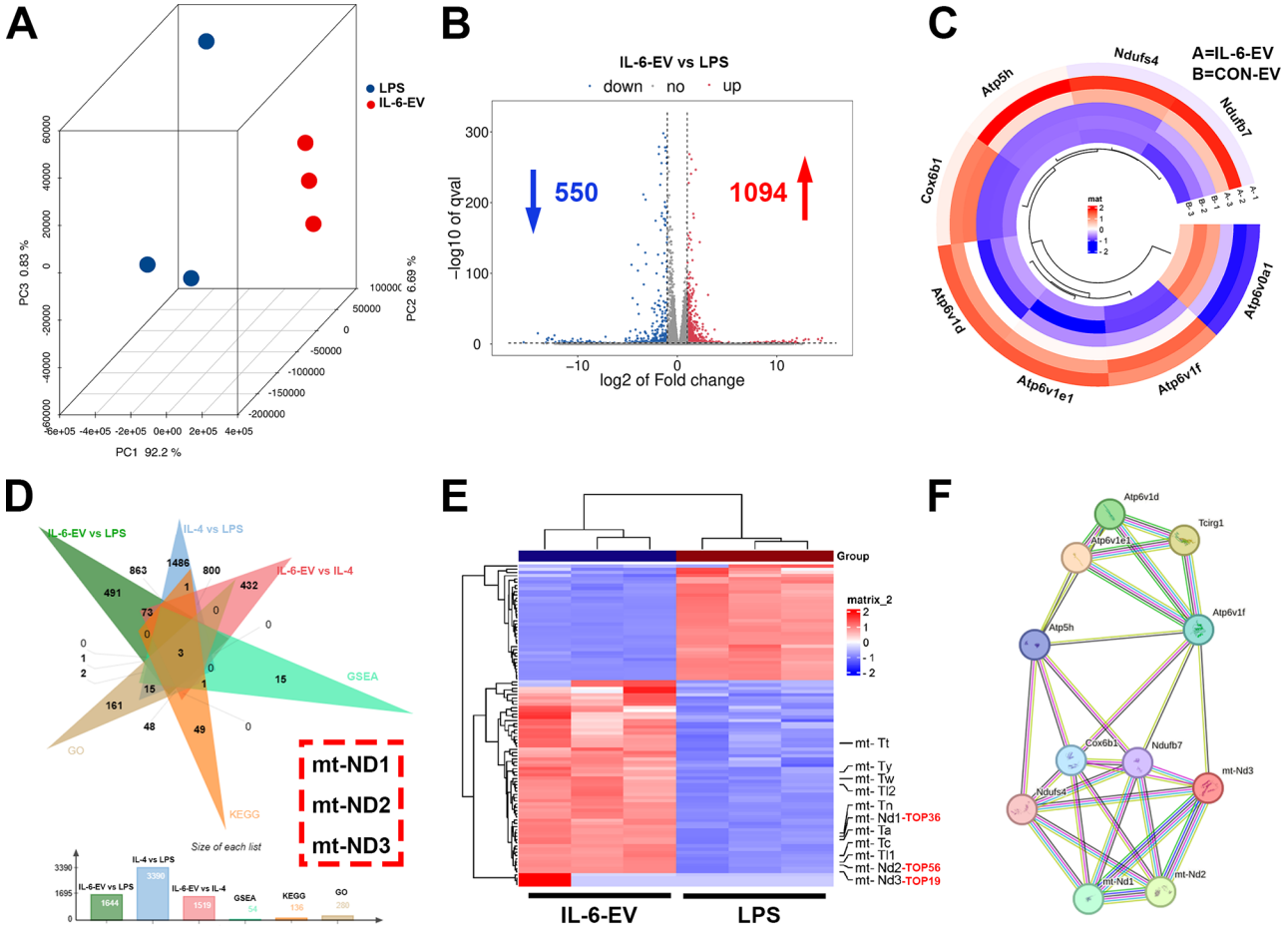

Fig. 6 Crosstalk of reprogrammed macrophages on chondrocytes. (**A**) Schematic illustration of the co-culture model featuring macrophages and chondrocytes. (**B**) Identification of primary chondrocytes. (**C**) COL II, ADAMTS5, and C-caspase3 among various groups investigated by Western blot. (**D-F**) Statistical analysis of COL II, ADAMTS5, and C-caspase3. (**G, H**) COL II and MMP13 among various groups investigated by Immunofluorescence staining and (**I, J**) statistical analysis of them. All data are shown as means ± standard deviations ($n = 3$), *$p < 0.05$, **$p < 0.01$, ***$p < 0.001$, ****$p < 0.0001$

from various databases (IL-6-EV vs. LPS, IL-6-EV vs. IL-4, IL-4 vs. LPS, KEGG, GO, and GSEA), identifying three genes: mt-ND1, mt-ND2, and mt-ND3 (Fig. 6D). As shown in Fig. 6E, clustering of highly expressed differentially expressed genes (FPKM > 1) revealed that mt-ND3 ranked 19th, mt-ND1 ranked 36th, and mt-ND2 ranked 56th among the 582 upregulated genes. Protein-protein interaction (PPI) network analysis predicted interactions between the eight oxidative phosphorylation proteins enriched in IL-6-EV (Fig. 6C) and the mt-ND1, mt-ND2, and mt-ND3 genes (Fig. 6F). These results suggest that IL-6-EV may regulate the expression of mt-ND1, mt-ND2, and mt-ND3 in macrophages, influencing the function of the mitochondrial electron transport chain (ETC, the site of OXPHOS), and ultimately controlling macrophage phenotype polarization.

IL-6-EV promotes the expression of mt-ND3 and ETC complexes in macrophages

To validate the results from macrophage the RNA sequencing analysis, we used qPCR to examine the expression of mt-ND1, mt-ND2, and mt-ND3 in macrophages. As shown in Fig. 7A-C, LPS treatment did not significantly affect the expression of mt-ND1 or mt-ND2 but significantly suppressed mt-ND3 expression. In contrast, IL-6-EV treatment significantly increased mt-ND3 expression compared to the LPS group, whereas CON-EV treatment had no significant effect on mt-ND3 expression. Therefore, we identified mt-ND3 as the key target for further exploration. Immunofluorescence and Western blot results (Fig. 7D-G) showed that LPS markedly inhibited mt-ND3 protein expression, whereas IL-6-EV significantly reversed this effect, consistent with the qPCR findings. mt-ND3 is a critical subunit of Complex I, closely related to its activity. We measured NADH-CoQ reductase activity as a proxy for Complex I activity. As shown in Fig. 7N, LPS significantly suppressed Complex I

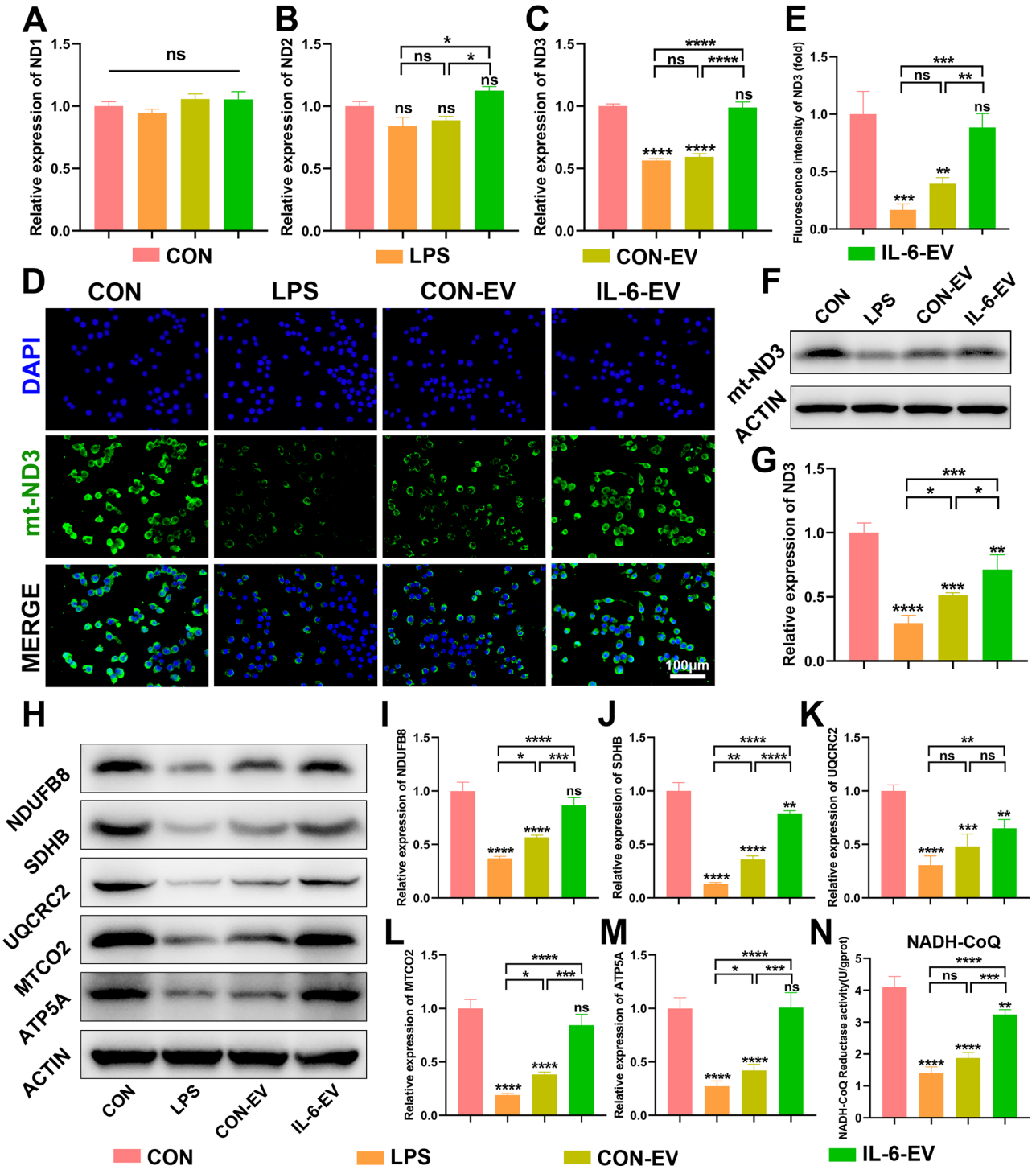

Fig. 7 Effects of CON-EV and IL-6-EV on mt-ND3 and OXPHOS in macrophages. (**A-C**) The expression of mt-ND1, mt-ND2, and mt-ND3 in macrophages investigated by qPCR. (**D**) The expression of mt-ND3 among different groups detected by immunofluorescence and (**E**) statistical analysis. (**F**) The expression of mt-ND3 among different groups detected by Western blot and (**G**) statistical analysis. (**H**) The expression of ETC Complexes I-V investigated by Western blot. (**I-N**) Statistical analysis of ETC Complexes I-V. All data are shown as means ± standard deviations ($n = 3$), *$p < 0.05$, **$p < 0.01$, ***$p < 0.001$, ****$p < 0.0001$

activity, whereas IL-6-EV treatment significantly attenuated this LPS-induced decrease. Complex I is the starting point of the ETC and the largest complex in the respiratory chain. After observing the effect of IL-6-EV on mt-ND3 expression and Complex I activity, we further examined its impact on the expression of ETC complexes (OXPHOS) in macrophages. Western blot results demonstrated that LPS inhibited the expression of ETC Complexes I-V, suggesting that LPS-induced M1 macrophage polarization also suppressed OXPHOS activity (Fig. 7H). While CON-EV treatment partially mitigated the LPS-induced reduction in Complexes I, II, IV, and V (Fig. 7I, J, L, M), it had no significant effect on Complex III. In contrast, IL-6-EV treatment significantly restored the expression of Complex III, as well as Complexes I, II, IV, and V (Fig. 7K, I, J, L, M). These findings suggest that in LPS-induced M1 macrophages, the expression of mt-ND3 and the activity of Complex I are suppressed, along with a downregulation of ETC Complexes I-V expression. Notably, IL-6-EV demonstrates a remarkable capacity to alleviate these alterations.

The mt-ND3/NADH-CoQ Axis as a key target for IL-6-EV to promote M2 macrophage polarization

To further elucidate the role of mt-ND3 in IL-6-EV-mediated M2 macrophage polarization, we used mt-ND3-siRNA (ND3-si) to knock down its expression in macrophages and observed the effects of IL-6-EV treatment. The results of qPCR (Fig. 8A) showed that ND3-si significantly inhibited the gene expression of mt-ND3, reducing it to 29% of the CON group($P<0.05$). Similarly, Western blot and qPCR results confirmed that ND3-si significantly decreased mt-ND3 protein levels (Fig. 8B, C). After silencing mt-ND3 expression, we examined mitochondrial Complex I activity and found that IL-6-EV's ability to enhance Complex I activity was significantly inhibited (Fig. 8M). Furthermore, as shown in Fig. 8D and E, after mt-ND3 knockdown, IL-6-EV could no longer increase the expression of NDUFB8, a subunit of Complex I ($p>0.05$ compared to the LPS group). Interestingly, ND3-si increased the expression of SDHB, a subunit of Complex II (Fig. 8D, F). Figure 8G-I show that ND3-si had no significant effect on the subunits of Complexes III, IV, and V compared to the IL-6-EV group. We then measured changes in ATP production in macrophages. As shown in Fig. 8N, after ND3-si was introduced, IL-6-EV could no longer counteract the LPS-induced decrease in ATP levels. Additionally, immunofluorescence analysis of macrophages (Fig. 8J-L) demonstrated that IL-6-EV significantly altered the expression of CD86 and CD206, but after the addition of ND3-si, the expression levels of these markers returned to baseline LPS group levels. These results suggest that IL-6-EV enhances Complex I activity by activating the expression of mt-ND3, improving oxidative phosphorylation and ATP production, and ultimately promoting macrophage polarization to the M2 phenotype.

IL-6-EV promotes OA cartilage repair

To evaluate whether IL-6-EV promote the repair and regeneration of cartilage in OA, we established a rat model of OA using ACLT and DMM. Four weeks post-surgery, the rats received intra-articular injections of PBS, CON-EV, or IL-6-EV (Fig. 9A). X-rays imaging was used to observe the knee joints of rats eight weeks after model induction. The results showed that, compared to the Sham surgery group, the joint space width in the PBS group was significantly narrowed ($P<0.05$), indicating substantial cartilage damage. The joint space width in the CON-EV group was also significantly narrowed ($P<0.05$), but showed some improvement compared to the PBS group ($P<0.05$). IL-6-EV treatment resulted in a significant improvement in cartilage damage, with joint space width noticeably wider than that in both the PBS and CON-EV groups ($P<0.05$), and no significant difference compared to the Sham group (Fig. 9B-D).

In addition to radiographic assessments, we conducted histological analyses using hematoxylin and eosin (HE) and Safranin O-fast green staining to evaluate cartilage changes. The results showed that the Sham group exhibited smooth, intact articular cartilage with evenly distributed cells and prominent staining of the cartilage extracellular matrix (ECM). In contrast, the PBS group exhibited severe cartilage erosion, thinning of the cartilage layer, and reduced ECM staining. The CON-EV group also showed substantial cartilage wear and significant loss of cartilage matrix. However, the IL-6-EV group exhibited smoother, more intact cartilage with evenly distributed cells, and ECM staining was noticeably stronger than in the PBS and CON-EV groups (Fig. 10A-B). We then assessed the severity of cartilage damage using the modified Mankin score. The results showed that the total Mankin scores, as well as the scores for structure, cells, and staining, were significantly lower in the IL-6-EV group compared to the PBS and CON-EV groups ($P<0.05$), with no significant difference from the Sham group (Fig. 10C-F), indicating that IL-6-EV significantly alleviated OA cartilage damage. We further examined the knee joint cartilage of OA rats with immunofluorescence staining. As shown in Fig. 10G-H, MMP13 expression was significantly higher in the PBS and CON-EV groups compared to the Sham group ($P<0.05$), whereas MMP13 expression in the IL-6-EV group was not significantly different from the Sham group. In the Sham group, Aggrecan expression was markedly higher, while its expression in the PBS group was significantly reduced ($P<0.05$). Although CON-EV partially restored Aggrecan expression, a significant difference remained compared to the

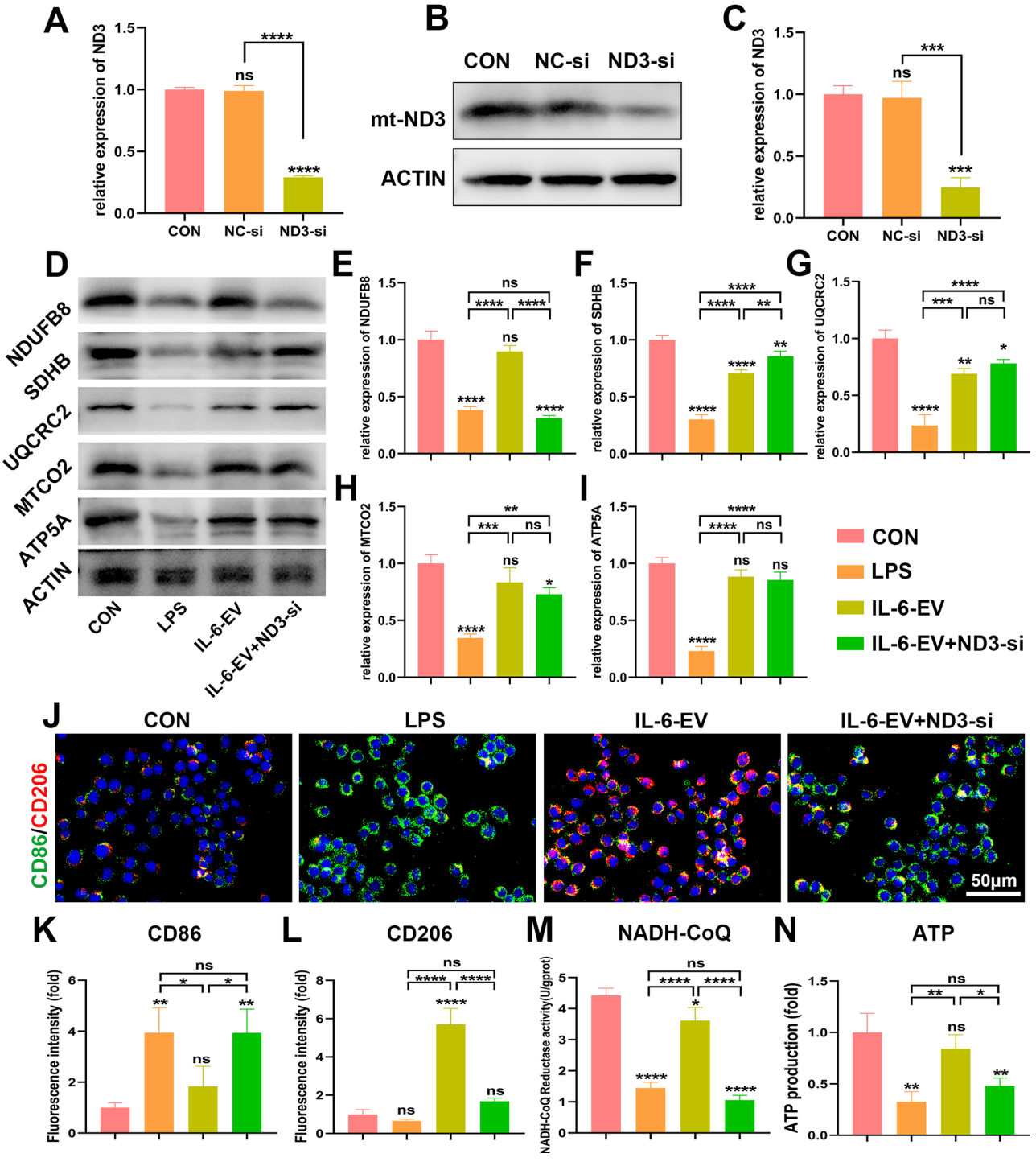

Fig. 8 The mt-ND3/NADH-CoQ axis is the key target for IL-6-EV to regulate mitochondrial OXPHOS and macrophage polarization. (**A**) The gene expression of mt-ND3 investigated by qPCR after negative control siRNA (NC-si) and mt-ND3-siRNA (ND3-si) transfection. (**B**) The protein expression of mt-ND3 investigated by Western blot after ND3-si transfection and (**C**) statistical analysis. (**D-I**) The protein expression of ETC Complexes I-V investigated by Western blot after ND3-si transfection and statistical analysis. (**J-L**) The expression of CD86 and CD206 detected by immunofluorescence after ND3-si transfection and statistical analysis. (**M**) Effect of ND3-si on NADH-CoQ reductase activity. (**N**) Effect of ND3-si on ATP production. All data are shown as means ± standard deviations ($n = 3$), $^{*}p < 0.05$, $^{**}p < 0.01$, $^{***}p < 0.001$, $^{****}p < 0.0001$

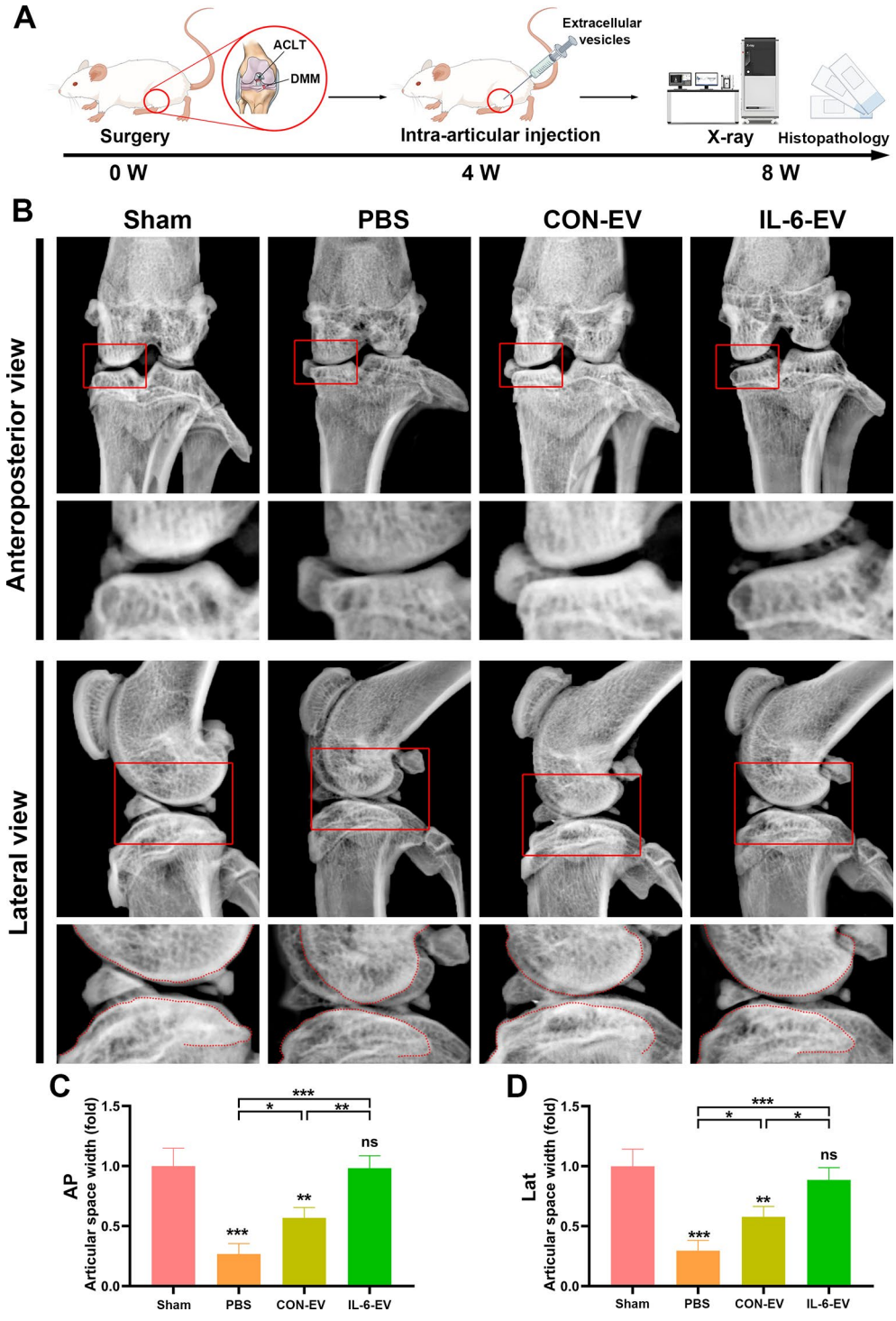

Fig. 9 Effects of CON-EV and IL-6-EV on the knee joint space width in rats. (**A**) Schematic diagram of experimental design in rats. (**B**) Anteroposterior and lateral radiographs of the knee joint in each group. (**C, D**) Statistical analysis of joint space width in the anteroposterior and lateral views. All data are shown as means ± standard deviations ($n = 5$), *$p < 0.05$, **$p < 0.01$, ***$p < 0.001$, ****$p < 0.0001$

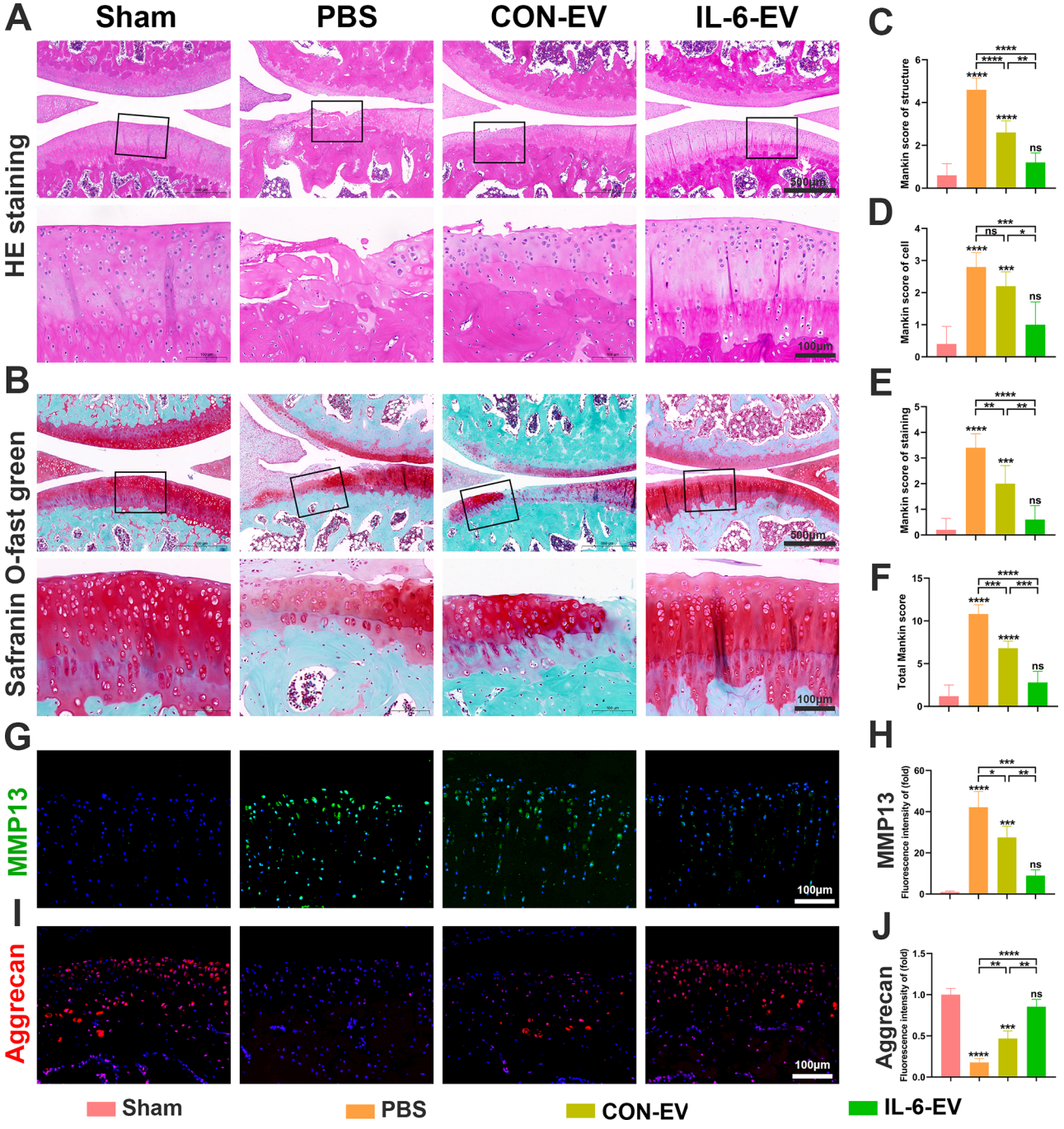

Fig. 10 Effects of CON-EV and IL-6-EV on cartilage degeneration in rats. (**A**) HE and (**B**) Safranin O-fast green staining of rat articular cartilage in each group at 8 weeks after surgery. (**C-F**) The structure, cell, staining, and total Mankin score of cartilage in each group. (**G, I**) Immunofluorescence staining and (**H, J**) statistical analysis of MMP13 and Aggrecan. All data are shown as means ± standard deviations ($n = 5$), *$p < 0.05$, **$p < 0.01$, ***$p < 0.001$, ****$p < 0.0001$

Sham group ($P < 0.05$). In contrast, IL-6-EV significantly increased Aggrecan expression compared to the PBS and CON-EV groups ($P < 0.05$) and showed no significant difference from the Sham group (Fig. 10I-J). These results are consistent with the X-ray findings, indicating that IL-6-EV can inhibit cartilage inflammation and promote the repair of OA cartilage.

IL-6-EV inhibits OA synovitis

Synovial inflammation is a key factor in the development and progression of OA. After demonstrating that IL-6-EV inhibits macrophage inflammation in vitro, we next aimed to assess its effect on synovitis in vivo. HE staining of synovial tissue showed that the Sham group exhibited a single layer of synovial lining cells, and the synovial

stroma exhibited normal cellularity with no inflammatory infiltrates. In contrast, the PBS group showed 4–5 layers of synovial lining cells, a significant increase in stromal cell density, and substantial inflammatory cell infiltration forming follicle-like structures. Both the CON-EV and IL-6-EV groups demonstrated significant improvements in synovial lining cell layers, stromal cell density and inflammatory infiltration compared to the PBS group (Fig. 11A). Pathological scoring of the synovial tissue (Fig. 11B) showed that the Sham group had a score of 6.80 ± 0.84, indicative of severe synovitis ($P < 0.05$). The CON-EV group scored 4.00 ± 1.22 (mild to moderate synovitis), representing a significant reduction compared to the PBS group, although remaining higher than the Sham group ($P < 0.05$). The IL-6-EV group scored 1.80 ± 1.30, showing no significant difference compared to the Sham group ($P > 0.05$). Immunohistochemistry results (Fig. 11C-D) indicated that the number of IL-6-positive cells in the PBS group was significantly higher than in the Sham group ($P < 0.05$). Treatment with CON-EV and IL-6-EV significantly reduced the proportion of IL-6-positive cells in the OA synovium, with IL-6-EV demonstrating superior effects compared to CON-EV ($P < 0.05$), suggesting that IL-6-EV significantly alleviates OA synovitis. Furthermore, immunofluorescence staining (Fig. 11E-G) revealed that IL-6-EV significantly inhibited iNOS expression in the OA synovium while enhancing CD206 expression, suggesting that IL-6-EV can inhibit M1 macrophage polarization and promote M2 macrophage polarization.

To further investigate the role of the mt-ND3 in IL-6-EV-mediated suppression of synovitis in vivo, we performed immunofluorescence staining for mt-ND3. The results (Fig. 11H-I) showed that mt-ND3 fluorescence intensity was significantly lower in the PBS group compared to in the Sham group ($P < 0.05$). Both the CON-EV and IL-6-EV groups exhibited significantly higher mt-ND3 fluorescence intensity compared to the PBS group ($P < 0.05$), with the mt-ND3 fluorescence intensity in the IL-6-EV group comparable to that of the Sham group ($P > 0.05$). These results suggest that IL-6-EV enhances mt-ND3 expression in synovial macrophages in vivo, promotes M2 macrophage polarization, and consequently reduces the severity of OA synovitis.

Discussion

Osteoarthritis (OA) is a disease that affects the entire joint; while multiple initial factors contribute to its onset, synovitis plays a central role in its progression [3]. Macrophages are the most abundant immune cells in the synovium and are strongly associated with synovial inflammation and OA severity [31]. Under physiological conditions, macrophages remain in a resting state. However, in OA, damage-associated molecular patterns (DAMPs) activate macrophages, inducing polarization into M1 macrophages that play a pro-inflammatory role and assist in debris clearance. Once the M1 phase of debris clearance is complete, it is essential for macrophages to promptly transition into M2 macrophages to exert anti-inflammatory and tissue repair functions [32]. If there is a blockade in the transition from M1 to M2, it may manifest as persistent inflammation in OA [33]. Therefore, regulating macrophage polarization balance represents a promising therapeutic target for OA. Mesenchymal stem cell-derived extracellular vesicles (MSCs-EVs) have significant immunoregulatory potential and are effective in modulating macrophage polarization balance, with the ability to enhance these capabilities through appropriate preconditioning [15]. In this study, the key difference from previous research is our innovative approach of using the "harmful" inflammatory factors present in the OA microenvironment to design a preconditioning strategy for MSCs, ultimately achieving a more effective treatment for OA. We demonstrated that preconditioning MSCs in the OA-specific microenvironment altered the protein profile of MSCs-EVs, enabling them to carry additional components involved in immune regulation and mitochondrial metabolism. Furthermore, our study revealed that IL-6-EV targets the mt-ND3/NADH-CoQ axis in macrophages, enhancing mitochondrial oxidative phosphorylation and thereby promoting M2 macrophage polarization. This novel mechanistic insight provides a new perspective on the potential of EV-based therapies for OA, offering promising avenues for future treatment strategies.

MSCs-EVs refer to particles released from cells, delimited by a lipid bilayer, that cannot replicate independently [34]. They can be considered modulators of intercellular communication, transferring lipids, nucleic acids (mRNA and microRNA), and cell-specific proteins between cells, thereby eliciting different cellular responses in recipient cells [35]. Importantly, the composition and function of MSCs-EVs are closely linked to the state of their parent cells [36]. Under physiological conditions, mesenchymal stem cells remain a low functional state, exhibiting phenotypic changes only upon stimulation by external factors [37]. This is reminiscent of the adaptive immune system's response to external stimuli, leading us to hypothesize whether MSCs possess a similar form of "immune memory." In this study, we observed that preconditioning MSCs with inflammatory factors (IFN-γ, IL-6, and TNF-α) highly expressed in OA synovial fluid led to an increased cargo of proteins involved in immune regulation and mitochondrial metabolism in the resulting EVs. Notably, IFN-γ, IL-6, and TNF-α are secreted by M1 macrophages and function as pro-inflammatory factors, contributing to the progression of inflammation and cartilage catabolism in the OA joint cavity [32].

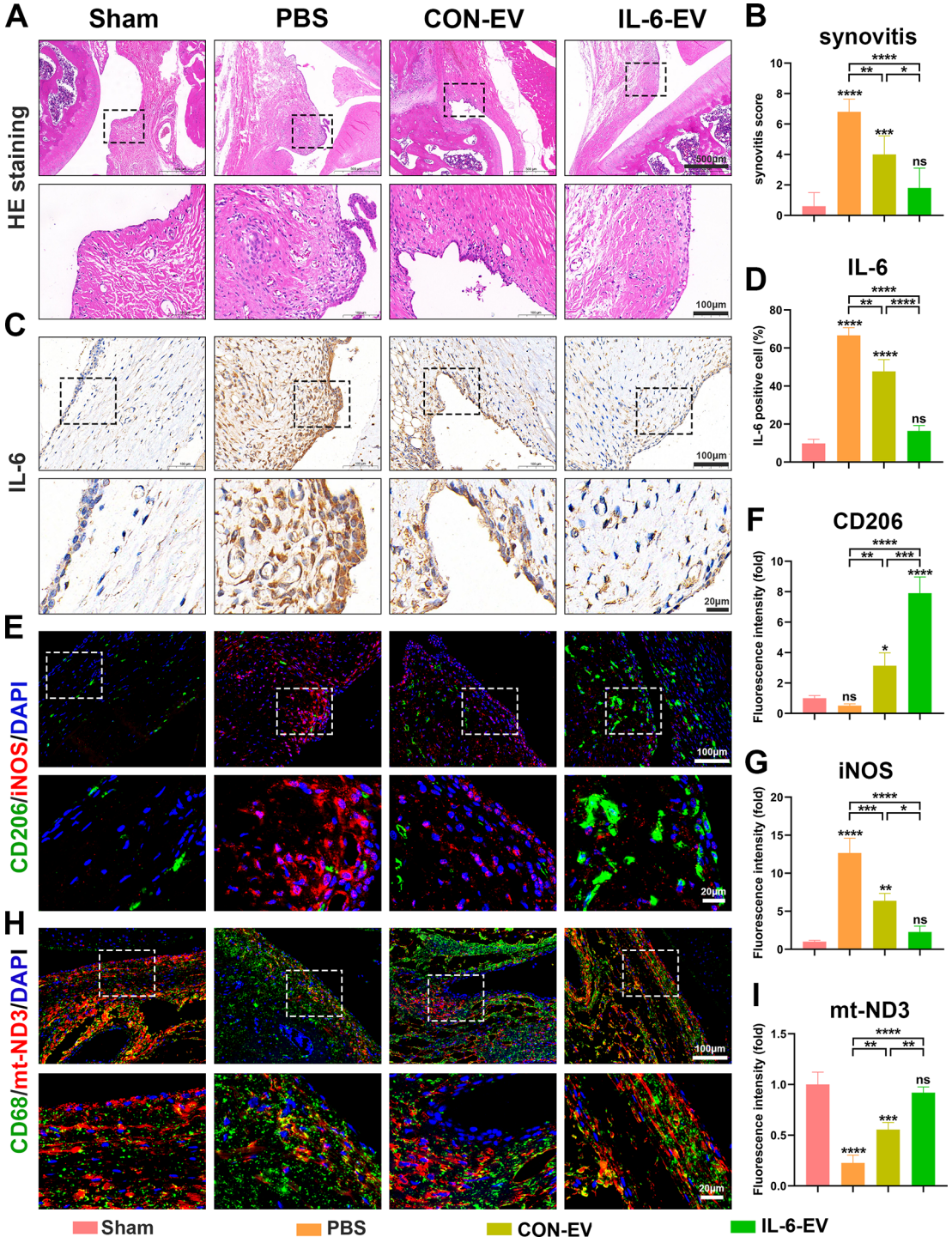

Fig. 11 Effects of CON-EV and IL-6-EV on synovitis and mt-ND3 in vivo. (**A**) HE staining of the synovium and (**B**) synovitis score in each group. (**C**) Immunohistochemical staining of IL-6 in the synovium and (**D**) statistical analysis. (**E**) Immunofluorescence staining and quantitative analysis of (**F**) CD206 and (**G**) iNOS in the synovium. (**H**) The expression of mt-ND3 in synovial macrophages from each group was detected by immunofluorescence. (**I**) Statistical analysis of mt-ND3 fluorescence intensity in vivo. All data are shown as means ± standard deviations ($n = 5$), $^{*}p < 0.05$, $^{**}p < 0.01$, $^{***}p < 0.001$, $^{****}p < 0.0001$

Interestingly, preconditioning MSCs with these factors in vitro enhanced the immunoregulatory capacity of the resulting MSCs-EVs. This is consistent with our prior research, which demonstrated that MSCs-EVs preconditioned with IFN-γ exhibited enhanced abilities to modulate OA inflammation [20]. Similarly, a study by Chen et al. confirmed that IFN-γ-preconditioned EVs effectively promote the polarization of M1 microglia to

M2 microglia [38]. Yuki Nakao et al. also demonstrated that EVs derived from TNF-α-treated human gingiva-derived MSCs enhance M2 macrophage polarization [18]. These findings further validate our hypothesis that MSCs possess a form of immune memory similar to that of the adaptive immune system: MSCs-EVs can function like specific antibodies in the adaptive immune system, providing a targeted "counterattack" against initial stimuli. On the other hand, among IFN-γ-EV, IL-6-EV, and TNF-α-EV, IL-6-EV appears to have a greater capacity to promote M2 macrophage polarization. This may be attributed to IL-6-EV carrying more proteins involved in mitochondrial metabolism, with KEGG pathways significantly enriched in oxidative phosphorylation. Oxidative phosphorylation refers to the biological process of generating ATP and H_2O within the mitochondrial electron transport chain, which is closely associated with macrophage phenotype reprogramming [39]. Studies have suggested that enhancing OXPHOS in macrophages can promote M2 polarization [28, 40], which may explain why IL-6-EV exhibits superior effects.

After investigating how the OA-specific microenvironment affects the proteomic composition of MSCs-EVs, we further focused on the impact of IL-6-EV on macrophage polarization and its underlying mechanisms. The metabolic hallmark of M1 macrophages is a shift from oxidative phosphorylation to aerobic glycolysis [41]. Enhanced glycolytic metabolism increases flux into the pentose phosphate pathway, providing more NADPH to drive NADPH oxidase and generate reactive oxygen species (ROS) [42]. Under these conditions, the electron transport process in the mitochondrial inner membrane is inhibited, reducing the proton gradient across the membrane, which decreases mitochondrial membrane potential, leading to increased ROS production and decreased ATP generation [43]. Moreover, recent studies in immunometabolism have shown that changes in mitochondrial structure and cristae morphology can directly influence macrophage polarization by altering energy metabolism [44, 45]. Our study found that when macrophages were polarized to the M1 phenotype by LPS induction, the changes in mitochondrial morphology and function aligned with these observations. Furthermore, IL-6-EV not only enhanced M1 macrophage polarization toward the M2 phenotype but also significantly improved mitochondrial structure and function. Therefore, we hypothesize that IL-6-EV may promote M2 macrophage polarization by enhancing OXPHOS in M1 macrophages. To test this hypothesis, we performed RNA sequencing on macrophages treated with LPS and IL-6-EV. By intersecting the differentially expressed genes with oxidative phosphorylation gene sets from the GSEA, GO, and KEGG databases, we identified three key genes: mt-ND1, mt-ND2, and mt-ND3. These genes ranked highly among the differentially expressed genes and interacted with the eight OXPHOS pathway proteins carried by IL-6-EV, suggesting that IL-6-EV may regulate these genes to promote M2 macrophage polarization. Mitochondria contain their own DNA (mtDNA), a circular, double-stranded DNA molecule 16.6 kb in length. They encode 13 proteins, 22 tRNAs and 2 rRNAs, all of which are essential components for mitochondrial energy metabolism [46]. The mt-ND1, mt-ND2, and mt-ND3 are mtDNA-encoded proteins and core subunits of ETC Complex I [47]. Complementary experiments following RNA sequencing analysis revealed that LPS-induced M1 macrophages did not show significant decreases in mt-ND1 or mt-ND2 expression; however, mt-ND3 expression was significantly suppressed by LPS and upregulated by IL-6-EV treatment. Moreover, we observed a consistent trend in the expression of mt-ND3 in macrophages, which paralleled the activity of Complex I (NADH-CoQ) and the expression patterns of ETC Complexes I-V. This finding underscores a potential correlation among these factors. After using siRNA to inhibit mt-ND3 expression in macrophages, the positive effects of IL-6-EV on Complex I expression, NADH-CoQ activity, ATP production, and M2 polarization were abrogated. This indicates that mt-ND3 is a crucial target through which IL-6-EV regulates mitochondrial function and macrophage polarization. Notably, inhibition of mt-ND3 did not reduce the expression of Complexes II-V; in fact, Complex II exhibited enhanced expression. This may be because Complex I and Complex II serve as two entry points into the ETC; when Complex I is inhibited, Complex II may compensate by increasing its expression and function. This suggests that a deficiency in mt-ND3 expression alone is sufficient to disrupt mitochondrial energy metabolism, reduce ATP production, and inhibit M2 macrophage polarization.

Complex I, also known as NADH-CoQ reductase, is the largest Complex in the respiratory chain and a major source of ROS [48]. Dysfunction in Complex I is closely associated with mitochondrial diseases and macrophage reprogramming [47]. In mammals, Complex I exists in both active and inactive states, with the inactive state resulting from reversible damage to the ubiquinone binding site [49]. Research has shown that mt-ND3 originates from the mitochondrial inner membrane and extensively interacts with hydrophilic domains. Cryo-electron microscopy studies have revealed that it is encircled by transmembrane helices (TMH), forming an mt-ND3-TMH1-2 loop positioned at the anterior of the structural domain. This loop restricts conformational changes at the hydrophobic/hydrophilic interface, a dynamically variable domain interface that serves as a crucial target for coupling ubiquinone reduction to proton translocation. Dysfunction of this interface impairs overall

Complex I function [50]. Previous studies have found that deficiency in the Ndufs4 protein, a core subunit of Complex I, enhances pro-inflammatory metabolic characteristics in macrophages and amplifies their response to LPS [51]. Other research has shown that mt-ND3 abnormalities can lead to decreased basal and maximal respiratory capacities in cells with Complex I deficiencies, and that MSCs can ameliorate such mitochondrial dysfunction [52]. These findings are consistent with our results, indicating that IL-6-EV enhances mitochondrial energy metabolism and promotes M2 macrophage polarization by regulating mt-ND3 expression and improving Complex I function.

Next, we investigated the effect of IL-6-EV-reprogrammed macrophages on IL-1β-induced chondrocytes inflammation. Consistent with previous studies, IL-1β disrupted the anabolic/catabolic balance of chondrocytes and induced apoptosis [53]. Macrophages reprogrammed by IL-6-EV (IL-6-EV-M2) effectively suppressed IL-1β-mediated chondrocytes inflammation and apoptosis while increasing COL II expression. Our results indicate that macrophages treated with IL-6-EV can improve chondrocyte homeostasis in a paracrine manner. As expected, once IL-6-EV induced macrophages to adopt an M2 phenotype, they secreted anti-inflammatory factors such as IL-10, which suppressed chondrocyte inflammation. This further confirms that IL-6-EV not only induced changes in macrophage surface markers (CD86/CD206) but also reprogrammed them into functional M2 macrophages capable of secreting anti-inflammatory factors.

Subsequently, we explored the therapeutic effects of IL-6-EV on synovitis and cartilage degeneration in a rat model of OA. X-ray imaging of joint space width can reflect the degree of cartilage damage and the severity of arthritis [54]. In this study, we observed that intra-articular injection of IL-6-EV significantly increased joint space width. Furthermore, histopathological analysis corroborated the radiological findings, showing that the OA model group exhibited thinning of the cartilage matrix, surface erosion of the cartilage, a reduced number of chondrocytes, disorganized chondrocyte arrangement, elevated MMP13 expression, and decreased Aggrecan content. Intra-articular injection of IL-6-EV effectively inhibited these changes, suggesting that IL-6-EV plays a protective role in preserving articular cartilage in vivo. The severity of synovitis is primarily assessed by the number of layers of synovial lining cells, stromal cell density, and inflammatory infiltration [29]. IL-6 is a major pro-inflammatory factor produced by M1 macrophages and serves as a marker of synovitis severity [32]. Our study revealed that IL-6-EV significantly inhibited OA synovitis in rats. The polarization imbalance between M1 and M2 macrophages is a critical factor in the onset and progression of synovitis [55]. Immunofluorescence analysis for iNOS (M1) and CD206 (M2) confirmed an increase in M1 macrophages in the OA group, while IL-6-EV significantly promoted M2 macrophage polarization in vivo, consistent with our in vitro findings. The inhibitory effect of IL-6-EV on OA synovitis and its protective effect on cartilage degeneration further suggest that IL-6-EV suppresses synovitis by regulating the polarization balance of macrophages, thereby reducing the secretion of inflammatory factors and protecting cartilage tissue. Additionally, we assessed the expression of mt-ND3 in macrophages in vivo. Our study revealed that during severe synovitis, the expression of mt-ND3 in synovial macrophages was significantly reduced, whereas IL-6-EV treatment notably increased mt-ND3 expression, aligning with the mechanistic results observed in our in vitro experiments. In summary, the in vivo results demonstrate the superiority of IL-6-EV in treating OA, as it promotes M2 macrophage polarization by enhancing mt-ND3 expression, thereby inhibiting synovitis and protecting articular cartilage.

Additionally, this study has several limitations. For instance, the mechanism by which IL-6-EV regulates mt-ND3 expression may involve epigenetic reprogramming of the gene or other mechanisms that were not explored in depth in our study. Furthermore, our study is not without the limitations that have persisted in previous EVs-based therapeutic strategies for diseases, namely, the inability to identify the specific components within the EVs responsible for the therapeutic effects. Although our study sequenced the protein profile of MSCs-EVs and showed complex interaction networks between the OXPHOS proteins and mt-ND3 through multi-omics analysis, we did not investigate the therapeutic effects of individual components.

Conclusion

In summary, this study illustrates that the OA-specific microenvironment preconditioning strategy enables MSCs to acquire a form of immune memory specific to OA, resulting in the secretion of MSCs-EV (IL-6-EV) that carry more components involved in immune regulation and energy metabolism. This preconditioning enhances their ability to promote M2 macrophage polarization, both in vivo and in vitro. Mechanistically, our findings suggest that IL-6-EV enhances mitochondrial oxidative phosphorylation in macrophages by regulating the mt-ND3/NADH-CoQ axis, thereby achieving the modulation of macrophage polarization and the treatment of OA. In conclusion, we have demonstrated the superiority of MSCs-EVs under the OA-specific microenvironment preconditioning strategy for OA treatment, offering novel insights for the clinical application of MSCs-EVs.

Abbreviations

OA	Osteoarthritis
MSCs	Mesenchymal stem cells
EVs	Extracellular vesicles
TNF-α	Tumor necrosis factor-α
IFN-γ	Interferon-gamma
IL-6	Interleukin-6
ROS	Reactive oxygen species
ATP	Adenosine Triphosphate
LPS	Lipopolysaccharide
DMEM	Dulbecco's modified eagle medium
ACLT	Anterior cruciate ligament transection
DMM	Destabilization of medial meniscus
TEM	Transmission electron microscopy
NTA	Nanoparticle tracking analysis
OXPHOS	Oxidative phosphorylation
ETC	Electron transport chain
MMP	Mitochondrial membrane potential
NC-si	Negative control siRNA

Supplementary Information

The online version contains supplementary material available at https://doi.org/10.1186/s12951-025-03216-1.

Supplementary Material 1

Acknowledgements

We would like to express our gratitude to the First Affiliated Hospital of Chongqing Medical University for their support of this study, as well as the editors and reviewers for their valuable comments on this research.

Author contributions

Jingdi Zhan and Jing Zou contributed equally to this work. Conceptualization：Jingdi Zhan, Jing Zou, Lili Dong, Wei Huang；Methodology and investigation: Jingdi Zhan, Jing Zou and Qiming Pang; Resources and data Curation: Zhuolin Chen and Junyan Liu; Software and validation: Jingdi Zhan, Senrui Liu, Chengcheng Du, Jiacheng Liu；Original Draft Preparation, review and editing: Jingdi Zhan, Jing Zou, Lili Dong and Wei Huang; Supervision and Project Administration: Weikang Zhao and Lili Dong；Funding Acquisition: Jingdi Zhan, Weikang Zhao, Lili Dong and Wei Huang. All authors read and approved the final manuscript.

Funding

This work was sponsored by the National Natural Science Foundation of China-Joint Fund Project (U22A20284); Natural Science Foundation of Chongqing, China (CSTB2022NSCQ-BHX0683); Postdoctoral Special Funding Project of Chongqing Human Resources and Social Security Bureau (2112012726787861); China Natural Science Foundation (82102571); China Postdoctoral Science Foundation(2022M710564); Doctoral Innovation Project of the First Affiliated Hospital of Chongqing Medical University (CYYY-BSYJSCXXM-202308).

Data availability

No datasets were generated or analysed during the current study.

Declarations

Ethics approval and consent to participate

The animal study was approved by the Ethics Committee of Chongqing Medical University (Approval Number: IACUC-CQMU-2024-0381).

Consent for publication

All the authors agreed to publish the study in the Journal of Nanobiotechnology.

Competing interests

The authors declare no competing interests.

Author details

[1]Department of Orthopedics, The First Affiliated Hospital of Chongqing Medical University, Chongqing, China
[2]Chongqing Municipal Health Commission Key Laboratory of Musculoskeletal Regeneration and Translational Medicine, The First Affiliated Hospital of Chongqing Medical University, Chongqing, China

Received: 28 October 2024 / Accepted: 10 February 2025
Published online: 25 February 2025

References

1. Katz JN, Arant KR, Loeser RF. Diagnosis and treatment of hip and knee osteoarthritis: a review. JAMA. 2021;325:568–78.
2. Hunter DJ, Bierma-Zeinstra S. Osteoarthritis. *Lancet* 2019, 393:1745–1759.
3. Lv Z, Yang YX, Li J, Fei Y, Guo H, Sun Z, Lu J, Xu X, Jiang Q, Ikegawa S, Shi D. Molecular classification of knee osteoarthritis. Front Cell Dev Biol. 2021;9:725568.
4. Orlowsky EW, Kraus VB. The role of innate immunity in osteoarthritis: when our first line of defense goes on the offensive. J Rheumatol. 2015;42:363–71.
5. Qin L, Yang J, Su X, Xilan L, Lei Y, Dong L, Chen H, Chen C, Zhao C, Zhang H, et al. The mir-21-5p enriched in the apoptotic bodies of M2 macrophage-derived extracellular vesicles alleviates osteoarthritis by changing macrophage phenotype. Genes Dis. 2023;10:1114–29.
6. Kraus VB, McDaniel G, Huebner JL, Stabler TV, Pieper CF, Shipes SW, Petry NA, Low PS, Shen J, McNearney TA, Mitchell P. Direct in vivo evidence of activated macrophages in human osteoarthritis. Osteoarthritis Cartilage. 2016;24:1613–21.
7. Li Y, Wang J, Qian D, Chen L, Mo X, Wang L, Wang Y, Cui W. Electrospun fibrous sponge via short fiber for mimicking 3D ECM. J Nanobiotechnol. 2021;19:131.
8. Hsueh YH, Buddhakosai W, Le PN, Tu YY, Huang HC, Lu HE, Chen WL, Tu YK. Therapeutic effect of induced pluripotent stem cell -derived extracellular vesicles in an in vitro and in vivo osteoarthritis model. J Orthop Translat. 2023;38:141–55.
9. Scruggs BA, Semon JA, Zhang X, Zhang S, Bowles AC, Pandey AC, Imhof KM, Kalueff AV, Gimble JM, Bunnell BA. Age of the donor reduces the ability of human adipose-derived stem cells to alleviate symptoms in the experimental autoimmune encephalomyelitis mouse model. Stem Cells Transl Med. 2013;2:797–807.
10. English K. Mechanisms of mesenchymal stromal cell immunomodulation. Immunol Cell Biol. 2013;91:19–26.
11. Kim DS, Jang IK, Lee MW, Ko YJ, Lee DH, Lee JW, Sung KW, Koo HH, Yoo KH. Enhanced Immunosuppressive properties of Human mesenchymal stem cells primed by Interferon-gamma. EBioMedicine. 2018;28:261–73.
12. Polchert D, Sobinsky J, Douglas G, Kidd M, Moadsiri A, Reina E, Genrich K, Mehrotra S, Setty S, Smith B, Bartholomew A. IFN-gamma activation of mesenchymal stem cells for treatment and prevention of graft versus host disease. Eur J Immunol. 2008;38:1745–55.
13. Esmaeili A, Hosseini S, Kamali A, Hosseinzadeh M, Shekari F, Baghaban Eslaminejad M. Co-aggregation of MSC/chondrocyte in a dynamic 3D culture elevates the therapeutic effect of secreted extracellular vesicles on osteoarthritis in a rat model. Sci Rep. 2022;12:19827.
14. Ren W, Hou J, Yang C, Wang H, Wu S, Wu Y, Zhao X, Lu C. Extracellular vesicles secreted by hypoxia pre-challenged mesenchymal stem cells promote non-small cell lung cancer cell growth and mobility as well as macrophage M2 polarization via mir-21-5p delivery. J Exp Clin Cancer Res. 2019;38:62.
15. Ferreira JR, Teixeira GQ, Santos SG, Barbosa MA, Almeida-Porada G, Goncalves RM. Mesenchymal stromal cell secretome: influencing therapeutic potential by Cellular Pre-conditioning. Front Immunol. 2018;9:2837.
16. Li M, Jiang Y, Hou Q, Zhao Y, Zhong L, Fu X. Potential pre-activation strategies for improving therapeutic efficacy of mesenchymal stem cells: current status and future prospects. Stem Cell Res Ther. 2022;13:146.
17. Chi H, Pepper M, Thomas PG. Principles and therapeutic applications of adaptive immunity. Cell. 2024;187:2052–78.
18. Nakao Y, Fukuda T, Zhang Q, Sanui T, Shinjo T, Kou X, Chen C, Liu D, Watanabe Y, Hayashi C, et al. Exosomes from TNF-alpha-treated human gingiva-derived MSCs enhance M2 macrophage polarization and inhibit periodontal bone loss. Acta Biomater. 2021;122:306–24.
19. Yao M, Cui B, Zhang W, Ma W, Zhao G, Xing L. Exosomal miR-21 secreted by IL-1beta-primed-mesenchymal stem cells induces macrophage M2 polarization and ameliorates sepsis. Life Sci. 2021;264:118658.

20. Liu S, Cheng S, Chen B, Xiao P, Zhan J, Liu J, Chen Z, Liu J, Zhang T, Lei Y, Huang W. Microvesicles-hydrogel breaks the cycle of cellular senescence by improving mitochondrial function to treat osteoarthritis. J Nanobiotechnol. 2023;21:429.
21. Xu H, Zhu Y, Hsiao AW, Xu J, Tong W, Chang L, Zhang X, Chen YF, Li J, Chen W, et al. Bioactive glass-elicited stem cell-derived extracellular vesicles regulate M2 macrophage polarization and angiogenesis to improve tendon regeneration and functional recovery. Biomaterials. 2023;294:121998.
22. Ning Y, Huang P, Chen G, Xiong Y, Gong Z, Wu C, Xu J, Jiang W, Li X, Tang R, et al. Atorvastatin-pretreated mesenchymal stem cell-derived extracellular vesicles promote cardiac repair after myocardial infarction via shifting macrophage polarization by targeting microRNA-139-3p/Stat1 pathway. BMC Med. 2023;21:96.
23. Tur J, Vico T, Lloberas J, Zorzano A, Celada A. Macrophages and mitochondria: a critical interplay between metabolism, signaling, and the functional activity. Adv Immunol. 2017;133:1–36.
24. Willenborg S, Sanin DE, Jais A, Ding X, Ulas T, Nuchel J, Popovic M, MacVicar T, Langer T, Schultze JL, et al. Mitochondrial metabolism coordinates stage-specific repair processes in macrophages during wound healing. Cell Metab. 2021;33:2398–e24142399.
25. Lloberas J, Munoz JP, Hernandez-Alvarez MI, Cardona PJ, Zorzano A, Celada A. Macrophage mitochondrial MFN2 (mitofusin 2) links immune stress and immune response through reactive oxygen species (ROS) production. Autophagy. 2020;16:2307–9.
26. Benmoussa K, Garaude J, Acin-Perez R. How mitochondrial metabolism contributes to Macrophage phenotype and functions. J Mol Biol. 2018;430:3906–21.
27. Zhan J, Yan Z, Kong X, Liu J, Lin Z, Qi W, Wu Y, Lin J, Pan X, Xue X. Lycopene inhibits IL-1beta-induced inflammation in mouse chondrocytes and mediates murine osteoarthritis. J Cell Mol Med. 2021;25:3573–84.
28. Xiao P, Han X, Huang Y, Yang J, Chen L, Cai Z, Hu N, Cui W, Huang W. Reprogramming macrophages via immune cell mobilized hydrogel microspheres for osteoarthritis treatments. Bioact Mater. 2024;32:242–59.
29. Krenn V, Morawietz L, Burmester GR, Kinne RW, Mueller-Ladner U, Muller B, Haupl T. Synovitis score: discrimination between chronic low-grade and high-grade synovitis. Histopathology. 2006;49:358–64.
30. Weinberg SE, Sena LA, Chandel NS. Mitochondria in the regulation of innate and adaptive immunity. Immunity. 2015;42:406–17.
31. Wu CL, Harasymowicz NS, Klimak MA, Collins KH, Guilak F. The role of macrophages in osteoarthritis and cartilage repair. Osteoarthritis Cartilage. 2020;28:544–54.
32. Zhang H, Cai D, Bai X. Macrophages regulate the progression of osteoarthritis. Osteoarthritis Cartilage. 2020;28:555–61.
33. Zhao K, Ruan J, Nie L, Ye X, Li J. Effects of synovial macrophages in osteoarthritis. Front Immunol. 2023;14:1164137.
34. Welsh JA, Goberdhan DCI, O'Driscoll L, Buzas EI, Blenkiron C, Bussolati B, Cai H, Di Vizio D, Driedonks TAP, Erdbrugger U, et al. Minimal information for studies of extracellular vesicles (MISEV2023): from basic to advanced approaches. J Extracell Vesicles. 2024;13:e12404.
35. Toh WS, Lai RC, Hui JHP, Lim SK. MSC exosome as a cell-free MSC therapy for cartilage regeneration: implications for osteoarthritis treatment. Semin Cell Dev Biol. 2017;67:56–64.
36. Kalluri R, LeBleu VS. The biology, function, and biomedical applications of exosomes. Science 2020, 367.
37. Guerrouahen BS, Sidahmed H, Al Sulaiti A, Al Khulaifi M, Cugno C. Enhancing Mesenchymal Stromal Cell Immunomodulation for Treating Conditions Influenced by the Immune System. *Stem Cells Int* 2019, 2019:7219297.
38. Chen C, Chang ZH, Yao B, Liu XY, Zhang XW, Liang J, Wang JJ, Bao SQ, Chen MM, Zhu P, Li XH. 3D printing of interferon gamma-preconditioned NSC-derived exosomes/collagen/chitosan biological scaffolds for neurological recovery after TBI. Bioact Mater. 2024;39:375–91.
39. Liu Y, Xu R, Gu H, Zhang E, Qu J, Cao W, Huang X, Yan H, He J, Cai Z. Metabolic reprogramming in macrophage responses. Biomark Res. 2021;9:1.
40. Wculek SK, Heras-Murillo I, Mastrangelo A, Mananes D, Galan M, Miguel V, Curtabbi A, Barbas C, Chandel NS, Enriquez JA, et al. Oxidative phosphorylation selectively orchestrates tissue macrophage homeostasis. Immunity. 2023;56:516–e530519.
41. Rodriguez-Prados JC, Traves PG, Cuenca J, Rico D, Aragones J, Martin-Sanz P, Cascante M, Bosca L. Substrate fate in activated macrophages: a comparison between innate, classic, and alternative activation. J Immunol. 2010;185:605–14.
42. West AP, Brodsky IE, Rahner C, Woo DK, Erdjument-Bromage H, Tempst P, Walsh MC, Choi Y, Shadel GS, Ghosh S. TLR signalling augments macrophage bactericidal activity through mitochondrial ROS. Nature. 2011;472:476–80.
43. Mills EL, Kelly B, Logan A, Costa ASH, Varma M, Bryant CE, Tourlomousis P, Dabritz JHM, Gottlieb E, Latorre I, et al. Succinate dehydrogenase supports metabolic repurposing of Mitochondria to Drive Inflammatory macrophages. Cell. 2016;167:457–e470413.
44. Kawano I, Bazila B, Jezek P, Dlaskova A. Mitochondrial Dynamics and Cristae shape changes during metabolic reprogramming. Antioxid Redox Signal. 2023;39:684–707.
45. Suomalainen A, Nunnari J. Mitochondria at the crossroads of health and disease. Cell. 2024;187:2601–27.
46. Gustafsson CM, Falkenberg M, Larsson NG. Maintenance and expression of mammalian mitochondrial DNA. Annu Rev Biochem. 2016;85:133–60.
47. Zickermann V, Wirth C, Nasiri H, Siegmund K, Schwalbe H, Hunte C, Brandt U. Structural biology. Mechanistic insight from the crystal structure of mitochondrial complex I. Science. 2015;347:44–9.
48. Okoye CN, Koren SA, Wojtovich AP. Mitochondrial complex I ROS production and redox signaling in hypoxia. Redox Biol. 2023;67:102926.
49. Zhu J, Vinothkumar KR, Hirst J. Structure of mammalian respiratory complex I. Nature. 2016;536:354–8.
50. Galkin A, Meyer B, Wittig I, Karas M, Schagger H, Vinogradov A, Brandt U. Identification of the mitochondrial ND3 subunit as a structural component involved in the active/deactive enzyme transition of respiratory complex I. J Biol Chem. 2008;283:20907–13.
51. Cai S, Zhao M, Zhou B, Yoshii A, Bugg D, Villet O, Sahu A, Olson GS, Davis J, Tian R. Mitochondrial dysfunction in macrophages promotes inflammation and suppresses repair after myocardial infarction. J Clin Invest 2023, 133.
52. Navaratnarajah T, Bellmann M, Seibt A, Anand R, Degistirici O, Meisel R, Mayatepek E, Reichert A, Baertling F, Distelmaier F. Mesenchymal stem cells improve redox homeostasis and mitochondrial respiration in fibroblast cell lines with pathogenic MT-ND3 and MT-ND6 variants. Stem Cell Res Ther. 2022;13:256.
53. Lei Y, Wang Y, Shen J, Cai Z, Zhao C, Chen H, Luo X, Hu N, Cui W, Huang W. Injectable hydrogel microspheres with self-renewable hydration layers alleviate osteoarthritis. Sci Adv. 2022;8:eabl6449.
54. Paixao T, DiFranco MD, Ljuhar R, Ljuhar D, Goetz C, Bertalan Z, Dimai HP, Nehrer S. A novel quantitative metric for joint space width: data from the Osteoarthritis Initiative (OAI). Osteoarthritis Cartilage. 2020;28:1055–61.
55. Zhang H, Lin C, Zeng C, Wang Z, Wang H, Lu J, Liu X, Shao Y, Zhao C, Pan J, et al. Synovial macrophage M1 polarisation exacerbates experimental osteoarthritis partially through R-spondin-2. Ann Rheum Dis. 2018;77:1524–34.

Publisher's note